

Recent progress on structural coloration

Yingjie Li,^{a,†} Jingtian Hu,^{a,†} Yixuan Zeng,^{a,†} Qinghai Song,^{a,b,*} Cheng-Wei Qiu,^c and Shumin Xiao^{a,b,d,*}

^aMinistry of Industry and Information Technology Key Lab of Micro-Nano Optoelectronic Information System, Guangdong Provincial Key Laboratory of Semiconductor Optoelectronic Materials and Intelligent Photonic Systems, Harbin Institute of Technology, Shenzhen, China

^bPengcheng Laboratory, Shenzhen, China

^cDepartment of Electrical and Computer Engineering, National University of Singapore, Singapore, Singapore

^dCollaborative Innovation Center of Extreme Optics, Shanxi University, Taiyuan, China

Abstract. Structural coloration generates colors by the interaction between incident light and micro- or nano-scale structures. It has received tremendous interest for decades, due to advantages including robustness against bleaching and environmentally friendly properties (compared with conventional pigments and dyes). As a versatile coloration strategy, the tuning of structural colors based on micro- and nanoscale photonic structures has been extensively explored and can enable a broad range of applications including displays, anti-counterfeiting, and coating. However, scholarly research on structural colors has had limited impact on commercial products because of their disadvantages in cost, scalability, and fabrication. In this review, we analyze the key challenges and opportunities in the development of structural colors. We first summarize the fundamental mechanisms and design strategies for structural colors while reviewing the recent progress in realizing dynamic structural coloration. The promising potential applications including optical information processing and displays are also discussed while elucidating the most prominent challenges that prevent them from translating into technologies on the market. Finally, we address the new opportunities that are underexplored by the structural coloration community but can be achieved through multidisciplinary research within the emerging research areas.

Keywords: structural coloration; metasurfaces; nanophotonics.

Received Jan. 17, 2024; revised manuscript received Mar. 6, 2024; accepted Mar. 20, 2024; published online Apr. 22, 2024.

© The Authors. Published by CLP and SPIE under a Creative Commons Attribution 4.0 International License. Distribution or reproduction of this work in whole or in part requires full attribution of the original publication, including its DOI.

[DOI: [10.3788/PI.2024.R03](https://doi.org/10.3788/PI.2024.R03)]

1 Introduction

Vision is one of the primary ways humans perceive the world and the perception of color is a crucial component of vision, influencing our cognition, emotions, and interaction with the surrounding world^[1]. The colors observed in the natural world can be categorized into two main types based on their underlying principles: (1) the chemical colors that reflect colors by selective absorption of specific wavelengths based on electronic transitions in the specialized chemical bonds of molecular substances and (2) structural colors that manipulate light of specific wavelengths via optical modes that can be tuned by the geometric shape, size, or arrangement of the material structures.

Figure 1 provides a brief comparison between typical chemical and structural colors. As shown in Fig. 1(a), the green color of plant leaves is produced by chlorophyll, where chlorin serves as the chromophore that absorbs light from all the visible spectrum except for the green wavelength^[2]. Typically, the colors produced by humans, such as those seen in pigments or dyes in daily life, fall into this category^[3,4]. Structural colors including butterfly wings^[5–7], bird feathers^[8], and beetle shells^[9] provide an extraordinary alternative that nature has evolved. As depicted in Fig. 1(b), chameleons^[10], for example, can modulate their skin colors by changing the spacings between the nanoparticles via contraction and expansion of the skin, shifting the absorption and reflection resonance wavelengths of their optical modes.

Despite their widespread use, chemical colors can exhibit limited stability in harsh conditions such as high temperature and ultraviolet radiation that can destroy the key molecular structures of the chromophores. Moreover, the synthesis of dyes

*Address all correspondence to Qinghai Song, qinghai.song@hit.edu.cn; Shumin Xiao, shumin.xiao@hit.edu.cn

[†]These authors contributed equally to this work.

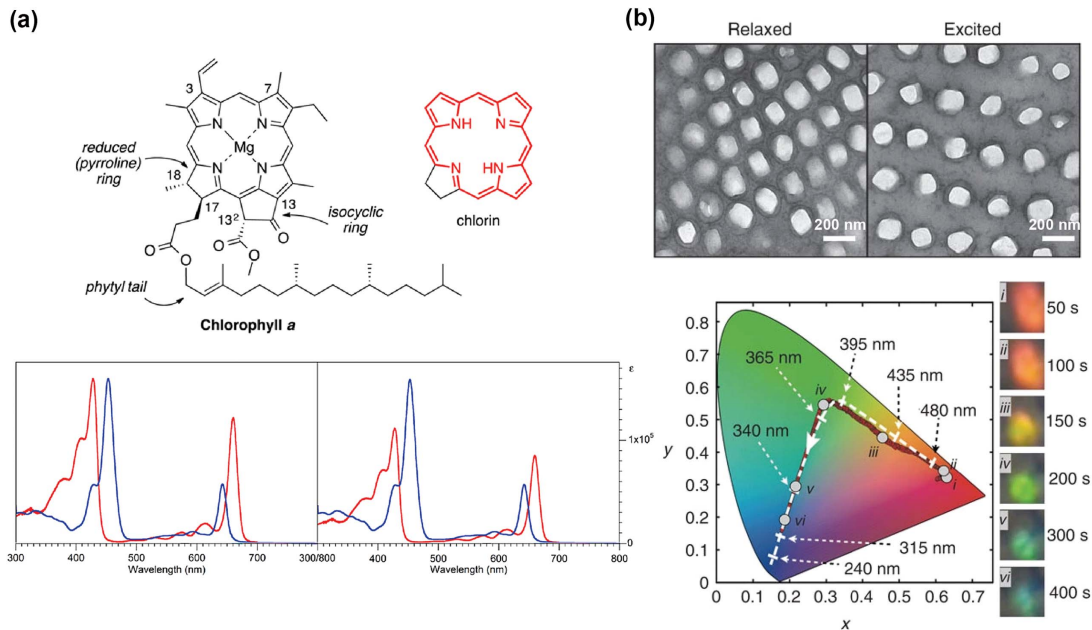


Fig. 1 Chemical and structural colors in nature. (a) Chemical structure of chlorophyll a and its chromophore chlorin, along with the absorption spectra of chlorophylls a and b in dichloromethane solution^[2]. (b) SEM image of nanostructures on the surface of chameleon skin and its color variation^[10].

involves multi-step chemical processes using toxic chemicals that pose significant issues and environmental concerns in the recycling process. Chemical colors, which cannot be patterned with high spatial resolution [less than 10^3 pixels per inch (PPI)]^[11,12], are also unsuitable for emerging display technologies that require extremely high pixel density. Structural colors provide a powerful alternative because they can be made from a wide range of materials (metals, dielectrics, and other materials)^[13–16], including the ones that not only exhibit strong robustness but also can be fabricated by clean and sustainable processes; for example, structural colors exhibit resistance to fading as long as the nanoscale structure remains intact. In particular, the nanofabrication techniques developed by the semiconductor industry also enable the precise production of structural colors with extremely high spatial resolution (over 10^5 PPI)^[17] and vivid colors, which has potential in augmented reality next microdisplays^[18–21].

In general, structural colors can be realized by nanophotonics systems ranging from multilayered thin films with engineered thicknesses to dielectric and/or metallic nanoparticles and the array they form. One-dimensional (1D) photonic crystals, formed by stacking multilayers of thin-film materials, realize the structural colors by prompting constructive and destructive interferences for photons with different wavelengths via the thin-film interference effect^[22–27], where the limited degrees of freedom of the multilayer film system constrains the variety of colors that can be realized^[28]. Additionally, changes in the angle of incidence of light can cause iridescence in multilayer pairs, which are often considered as undesirable display artifacts for common applications. Alternatively, self-assembly of nanospheres that exhibit photonic resonance is an effective way to achieve structural colors^[29–32]. Although self-assembled structures provide a simple means of fabrication, it is difficult to

achieve precise regulation of the various degrees of freedom of the structure to achieve desirable color effects.

Metasurfaces^[33–41]—planar structured materials with rationally designed, subwavelength-scale building blocks—have enabled precise control of light with high design flexibility. The metasurface's design freedom allows for amplitude modulation across the entire visible wavelength band, resulting in a wide color gamut with complete spectral coverage. Structural colors based on metasurfaces tend to achieve narrower spectral linewidths (which is important for RGB mode), higher efficiencies, and more saturated color properties than multilayered thin films and self-assembled systems. Due to the easy fabrication and the strong modulation of electromagnetic waves by plasmonic resonances, plasmonic metasurfaces made of metallic materials have realized structural coloration through excitation of localized surface plasmon resonances, which can achieve structural color with extremely high resolution beyond the diffraction limit^[42]. However, the plasmonic mode can also increase the optical absorption of metals at resonant wavelengths, which reduces the brightness of colors and the efficiency of light reflection and transmission. Therefore, lossless dielectric metasurfaces based on the Mie resonance have also been widely studied in the field of structural colors. Numerous high-performance structural colors for metasurfaces have been designed through these studies. However, once prepared, metasurfaces are often not adjustable so that the colors and patterns on the surface are fixed and cannot be used for dynamic displaying of visual information.

To facilitate the development of next-generation display technology that targets high resolution and vivid color, research on achieving dynamically tunable structural colors is becoming the primary goal of the field and receives tremendous interest. Because structural colors arise from the interaction between materials and light at subwavelength scales, they can be tailored

in two ways: (1) by manipulating the optical properties of the material through external stimuli, such as using liquid crystals^[43,44] and phase change materials^[45,46], and (2) by reconfiguring the building blocks of the structural color by methods such as mechanical stretching of the substrate^[47,48].

As a field that has developed over several decades, structural colors have gradually found applications in various domains. Given the stringent requirements of micro displays for integration and resolution, structural colors have been widely explored as the foundation for the next generation of micro display devices. Apart from their application in conventional color displays, structural colors find extensive use in optical information storage due to their high spatial resolution and superb polarization tunability^[49–53]. Owing to the unique response of nanostructures to the light field, structural colors are employed in optical encryption and steganography, providing enhanced security features at the nanoscale^[54–56]. Furthermore, the metasurface offers extensive design flexibility and can be intelligently crafted to achieve multidimensional manipulation of the light field. This allows for simultaneous control of both amplitude and phase, resulting in a diverse range of structural colors and holographic displays^[57,58]. Moreover, numerous studies have applied structural colors to coatings and inks to provide clean and highly color-capable displays^[59–64]. In the realm of dynamic structural colors, their precise response to external stimuli positions them as visual sensing devices, opening avenues for real-time and passive sensing applications^[65,66]. Among these applications, the use of structural colors as biosensors has garnered widespread attention, offering capabilities such as visualization, simplified processes, and rapid or even real-time monitoring^[67,68].

In this review, we initially present the research progress of metasurfaces based on metal and dielectric materials in the field of structural coloration. Additionally, optimization algorithms and machine learning are considered the way forward for rapid metasurface design due to the difficulty of designing and optimizing metasurfaces with multi-parameter complex structures. We showcase the design methodologies for structural color metasurfaces aided by optimization algorithms and machine-learning techniques. This approach has the potential to substantially enhance color performance and design speed. Next-generation near-eye micro displays require high spatial resolution. However, existing display technologies face bottlenecks in resolution. Therefore, dynamically adjustable structured color displays are a strong contender for next-generation displays. We summarize the advancements in the research of dynamic and tunable metasurfaces for structural color, focusing on techniques involving phase change materials, liquid crystals, and flexible substrate deformations. In the extensive research on metasurface-based structural colors over the years, their unique properties have led to applications across various domains. Therefore, we will focus on highlighting the recent applications of metasurface-based structural colors in different fields, including displays, optical security, multidimensional information transmission, structural color coatings, and sensing. The practical applications of structural colors are poised to bring about widespread changes in everyday life. Additionally, we discuss future directions and opportunities in the field of structural colors, as well as the challenges in processing structural colors for commercialization and how to address them. This review also explores new and unexplored boundaries of the structural color field by combining it with new frontiers. Finally, we summarize the key findings of the review and offer insights into future directions.

2 Static Structural Colors

Structural color is the visual result under the combined action of refraction, diffraction, interference, and reflection caused by nano-scale structure. This section analyzes the main optical systems for producing structural color ranging from localized surface plasmon resonance (LSPR) to Mie resonance while introducing their mechanisms and unique advantages, which have made profound impacts in materials science, physics, chemistry, and biology. For structural coloration using metallic nanostructures, the ability to manipulate surface plasmons (SPs) in visible frequencies is original and contains tremendous latent capacity for new imaging and display technologies. In the simplest case, a single metal nanoparticle is excited by an external electromagnetic wave of a specific frequency, inducing a resonance of free electrons within the metal and exciting an electric field inside the structure. Metal nanostructures have been designed in various ways based on their plasmonic resonance mode, such as arrays of nano-discs and gap plasmonic modes consisting of very thin dielectric spacer layers, as illustrated in Fig. 2(a). However, the reflective mode and low efficiency limit more extensive application scenarios. Similar to a single metallic nanostructure, dielectric nanostructures can be excited by electromagnetic waves of appropriate wavelengths to form a toroidal electric field around the structure, which in turn excites a magnetic field inside the structure with significantly lower optical losses (compared to metals), as depicted by Fig. 2(b). Furthermore, photonic crystals possess a local mode known as the bound states in the continuum (BIC), which exhibit an extremely high-quality factor. This property is anticipated to be utilized in the development of structured color displays with exceptional performance. In order to achieve bright colors with high saturation, dielectrics-based structural colors are brought up and open up new opportunities of both fundamental and practical interests.

2.1 Plasmonic-Based Structural Colors

When light of a specific wavelength impinges on a metal surface, the phenomenon of collective oscillation between the free electrons on the metal surface and photons is known as SPs^[69]. SPs exhibit a strong near-field enhancement effect and in-plane momentum. With the rapid development of micrometer and nanometer manufacturing processes, subwavelength nanostructures based on SP have been successfully fabricated. In the field of nanophotonics, the plasmonic metasurface has become a transformative technology, enabling unprecedented control of light at the nanoscale^[70,71]. These two-dimensional arrays composed of nanostructured metal elements exploit the unique optical properties of plasmonic materials, especially noble metals like gold (Au) and silver (Ag)^[72,73]. Plasmonic metasurfaces can manipulate surface plasmon resonance (SPR), achieving precise control over the phase, amplitude, and polarization of light^[74–77]. This level of control has paved the way for numerous applications, including waveguides^[78,79], metalenses^[80], holography^[81], and wavefront modulation^[82,83]. One particularly fascinating application is the realization of structural color^[69].

Throughout history, people have known that metal nanoparticles can produce remarkable colors. Over 1700 years ago, Roman artisans created the famous Lycurgus Cup^[84] by mixing nano-sized metal particles into glass. Due to the strong modulation effect of SPR on electromagnetic waves, there have been numerous reports of high spatial resolution color filters based on

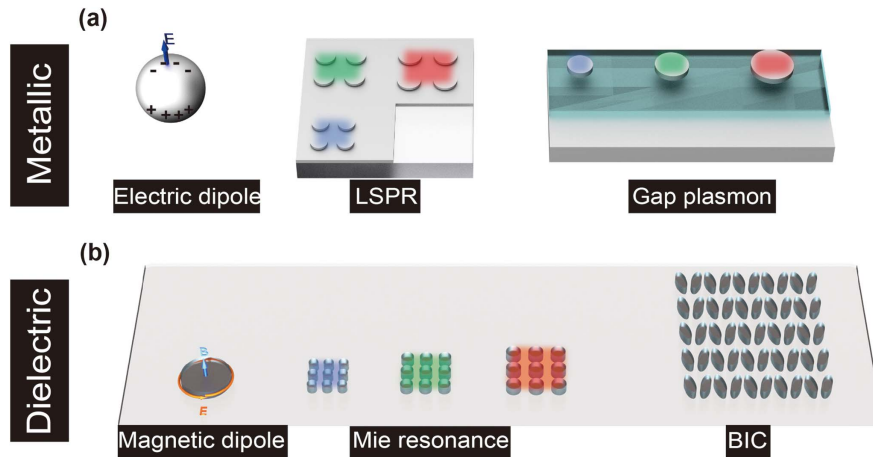


Fig. 2 Physical model for producing structural color. (a) Electric dipole response of single metal nanosphere; schematic representation of color response of blue, green, and red achieved by arrays of metal nanodisks of different sizes and periods; model of metasurface achieving gap plasmonic mode. (b) Magnetic dipole response of a single dielectric nanodisk; schematic representation of the color response of blue, green, and red achieved by arrays of dielectric nanodisks of different sizes and periods; schematic representation of a metasurface capable of generating BIC modes.

SPR^[49,85,86]. In addition to classical plasmonic metasurfaces, researchers have also designed new nanostructures such as gap plasmons^[87] and Fabry-Pérot (FP) cavities^[88–90], and this section will briefly discuss them.

In the past decade, structural colors based on metal metasurfaces have been extensively researched. In the early stages, structural colors of metal nanostructures with different geometric shapes, materials, and arrangements were widely investigated^[91–97]. Transmission-type structural colors were achieved using metal grating structures through a subtractive method or by employing metal nano-hole arrays with different shapes and periods for transmission-based RGB colors^[98]. Additionally, reflective structural colors based on metal nanostructures, such as nanodisks made of Au or Ag, demonstrated vibrant color displays with only a 2×2 array due to the strong LSPR effect,

as shown in Fig. 3(a)^[42]. Reflective structural colors were also achieved using anisotropic nano-hole structures, as illustrated in Fig. 3(b), where a cross-shaped hole array on a 100 nm thick aluminum (Al) film exhibited color responses under different polarizations^[99]. While structural color design based on metal structures allows for ultrahigh spatial resolution (over 1.2×10^5 PPI)^[100], challenges such as achieving high brightness, wide color gamut distribution, and process complexity remain unresolved, significantly limiting the practical applications of metal metasurface structural colors. In recent years, researchers have addressed these challenges by proposing innovative structural designs and process solutions.

Hail *et al.* designed an RGB structural color based on a plasmonic nanorod array, where the nanorods, composed of Ag, had a longitudinal axis in the y-direction with a periodicity

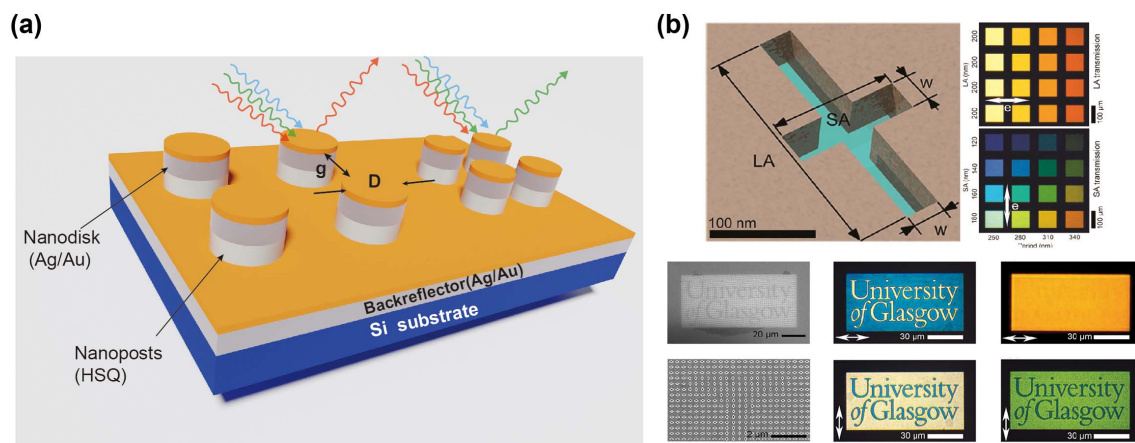


Fig. 3 Early designs of structural colors based on metal nanostructures. (a) Reflective structural color achieved with an array of Ag nanorods, requiring only a 2×2 array for distinguishable pixels^[42]. (b) Anisotropic cross-shaped nanoapertures for polarization-sensitive transmissive structural color^[99].

of $P_x = \lambda/n$ along the x-direction. Color tuning was achieved by adjusting the dimensions and periodic parameters of the nanorods, as illustrated in Fig. 4(a) (1)^[101]. Furthermore, at a fixed periodicity, simple control over nanorod size enabled independent adjustments in color brightness, as depicted in Fig. 4(a) (2). Figure 4(a) (3) demonstrates the blended spectra produced by mixing different primary color nanostructures, showcasing the potential for an infinite color palette through precise control of nanostructures. This design allows for ultra-smooth transitions in both color and brightness.

Xu and coworkers achieved high-performance plasmonic structural color through plasmonic resonance, manifesting an enhanced 90° optical rotation due to birefringence^[102]. The meta-pixel is designed as an anisotropic nanogroove array embedded in an optically thick silver film, as shown in Fig. 4(b) (1). In experiments, Si mold was initially prepared using traditional electron beam lithography (EBL) and reactive ion etching (RIE). Subsequently, an Ag layer was deposited on the Si template, and the desired samples were obtained after peeling. The prepared Si mold can be reused for a long time and is suitable for large-scale industrial production. The standard structural parameters of the nanogrooves are set to length (l) = 200 nm, width (w) = 60 nm, thickness (h) = 40 nm, and period (p) = 160 nm. The resonance wavelength is controlled by adjusting the structural parameters using a scaling factor (s). Figure 4(b) (2) displays the reflection cross-polarized spectra with S factors ranging from 1.0 to 2.65, covering the entire visible spectrum. Additionally, the color brightness of this plasmonic metasurface can be independently controlled by adjusting the rotation angle α between incident linearly polarized (LP) light and nano-grooves, as shown in Fig. 4(b) (3). Due to the sensitive response to orthogonally polarized light, as shown in Fig. 4(b) (4), the authors further applied it to advanced optical steganography. Using non-oriented nanogrooves to graphically represent information, specific information can only be read by specific incident LP light and a polarization analyzer, achieving advanced optical encryption. However, despite the high-performance structural color achieved by this plasmonic metasurface using polarization conversion, it is severely hindered by the requirement for LP light and a

polarization analyzer. Another noteworthy issue is its sensitivity to the incident angle, severely limiting its practical applications.

Furthermore, the FP cavity structure formed by sandwiching a dielectric material between two metal films has been widely studied as a relatively simple structure in the field of structural colors^[88,103–108]. In general, the transmission and reflection modes of FP cavities are typically determined by the phase shift propagated within the cavity, and this phase shift is influenced by the refractive index of the dielectric material, the thickness of the dielectric layer, and the angle of incident light. Therefore, various colors across the entire visible spectrum can be easily achieved by adjusting the thickness of the dielectric layer. However, due to the fact that the angle of incidence changes the path of light in the FP cavity, it exhibits different resonant wavelengths at different angles of incidence and rainbow colors in color, resulting in small observation angles.

To overcome the problem of different colors corresponding to different FP cavity lengths, Wei *et al.* embedded Si nanostructures into a FP cavity, achieving tunable transmission structural colors across the entire visible spectrum within a fixed cavity length^[109]. The structure, as shown in Fig. 5(a) (1), consisted of a Si nanoblock array encapsulated by two layers of 35 nm thick Ag films filled with PMMA. Control over the geometric dimensions and periodicity of the Si nanoblocks allowed for precise tuning of the response wavelength, resulting in a color gamut covering 194% of sRGB. Additionally, the mixing of nanostructures with different sizes enabled color blending capabilities, as illustrated in Fig. 5(a) (2). Furthermore, the embedded nanostructures introduced flexible polarization control, allowing for polarization-multiplexed FP structural colors by adjusting the responses of meta-atoms to different polarizations, as depicted in Fig. 5(a) (3).

Recently, Mohamed *et al.* designed a structure called Fabry-Perot resonance optical coatings (FROCs)^[110]. They deposited a layer of absorbing dielectric material on an FP cavity, where the absorbing medium forms a broadband absorbing cavity with the first metal layer, and the lower three layers form an FP resonance serving as a narrowband absorbing cavity. The coupling between the two resonant cavity modes exhibits Fano

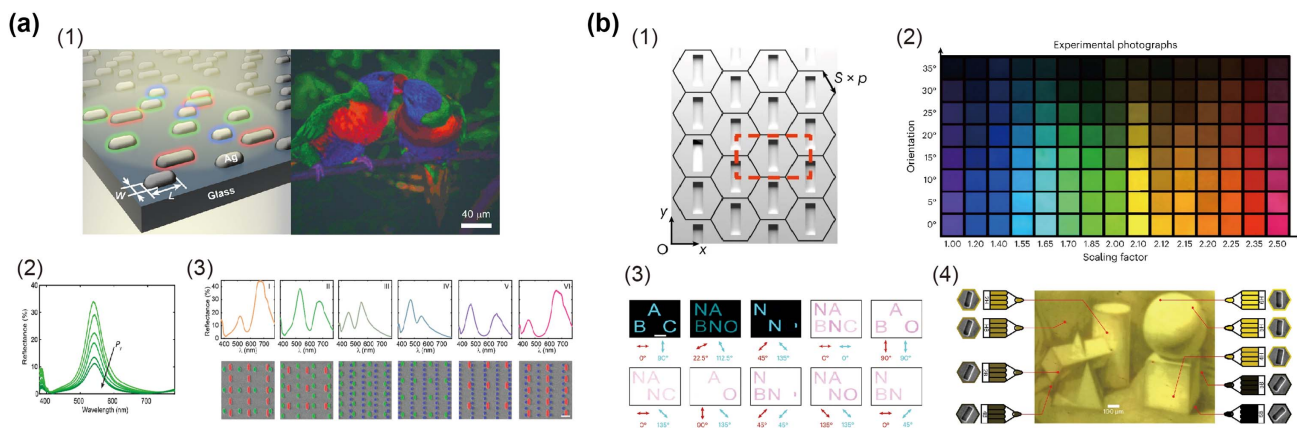


Fig. 4 Plasmonic structural color design for high-performance display. (a) Design using Ag nanorods for high-color saturation display (1), brightness control by adjusting nanorod size (2), and color tuning through the arrangement of structures with different wavelength responses (3)^[101]. (b) Schematic of high-performance structural color based on Ag nano-grooves for achieving complete control over brightness and color (1), (2), application of polarization response for advanced optical steganography (3), and achieving soft color displays through brightness variation (4)^[102].

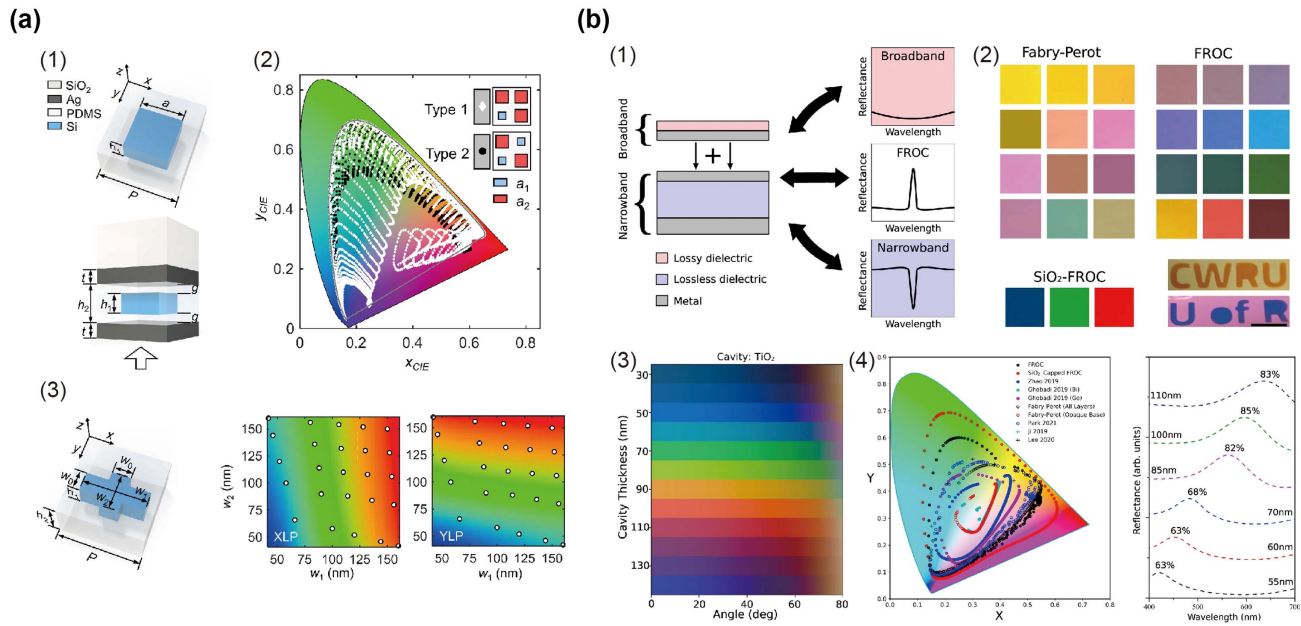


Fig. 5 Structural color design based on FP cavity. (a) Integration of Si nanostructures into FP cavity for uniform cavity length structural color display (1), color tuning through the mixture of different nanostructures on a high-color-saturation display foundation (2), and easy achievement of polarization response by controlling the symmetry of nanostructures (3)^[109]. (b) Schematic structure of FROCs formed by two coupled light absorbers (1), deposition of an absorbing medium on the FP cavity, coupling of the upper broadband mode with the lower FP resonance to form Fano resonance, resulting in vivid structural colors (2), (4), and exhibiting over 50° observation angle (3)^[110].

resonance, as shown in Fig. 5(b) (1). The optimized structure of FROCs consists of a 15 nm thick germanium (Ge) lossy layer, a 20 nm thick Ag layer, a TiO₂ lossless layer, and a 100 nm Ag layer from top to bottom. The thickness of the TiO₂ dielectric layer increases from 30 to 130 nm, achieving visible light coverage of the resonant wavelength. To further suppress the reflection at shorter wavelengths, a 50 nm layer of SiO₂ was deposited on top of FROCs as a refractive index matching layer, achieving a 61% coverage of the CIE color space. The colors and CIE coordinates for FP cavities, FROCs, and FROCs with deposited silica are shown in Figs. 5(b) (2) and 5(b) (3). In contrast to the structural colors of FP cavities, FROCs exhibit reflective colors over a larger range of observation angles, demonstrating significant color stability from 0° to 50°, as depicted in Fig. 5(b) (4). The design of FROCs solves the problem of poor color saturation and small observation angle in FP cavities, and amorphous silicon can be used to replace Ge as the absorption layer, and the metal layer in the structure can be used as the electrode to achieve color photovoltaic cells.

On the basis of the FP cavity, further patterning the top metal film forms a nanostructure array, allowing for the adjustment of structural colors through the shape and size of the nano-units^[89,111,112]. The top metal nanostructures, in conjunction with the ultra-thin dielectric layer, constitute a metal-insulator-metal (MIM) structure that exhibits gap plasmons. This phenomenon arises due to the strong near-field coupling between the plasmonic modes of the top nanostructures and the bottom metal film. Increasing the thickness of the dielectric spacer weakens the near-field coupling, causing the gap plasmon mode to degenerate into LSPR and FP resonance modes.

Miyata *et al.* designed a subwavelength color pixel structure based on an aluminum (Al) MIM plasmonic nanoantenna^[113]. As illustrated in Fig. 6(a) (1), the structure consists of a 100 nm thick Al film at the bottom, a 30 nm thick aluminum oxide (Al₂O₃) dielectric layer in the middle, and Al nanocylinders (height 40 nm) at the top. The color strongly depends on the diameter of the nanocylinders, as depicted in Fig. 6(a) (2). They further combined nanostructures with different diameters into a unit cell to achieve a black subwavelength pixel. Using a single nanopillar, they demonstrated the printing of structural colors to form the word “Nano,” as shown in Fig. 6(a) (3).

Blake *et al.* designed a subtractive color reflection structural color based on the gap plasmon mode^[114]. They utilized a hole-mask colloidal lithography (HCL) method to fabricate the top-layer nanodisk structures, achieving a large-area preparation process for reflective cyan, magenta, and yellow (CMY) structural colors, as illustrated in Fig. 6(b) (1). The self-assembly of colloids in HCL resulted in non-periodic distribution of Ag nanodisks as the top layer, a 30 nm thick Al₂O₃ spacer, and an Ag reflector as the bottom layer. Optimizing the structural parameters, they achieved vibrant and high-brightness reflective subtractive structural colors in cyan, magenta, and yellow. SEM images, reflection spectra, and CIE color coordinates are presented in Fig. 6(b) (2).

Overall, metal-plasmon-based structural colors have been a focal point of research in recent years, offering unique and vibrant coloration possibilities. In the pursuit of overcoming limitations associated with traditional pigments and dyes, researchers have explored the intricate interaction between metals and light. The use of metal nanostructures, such as

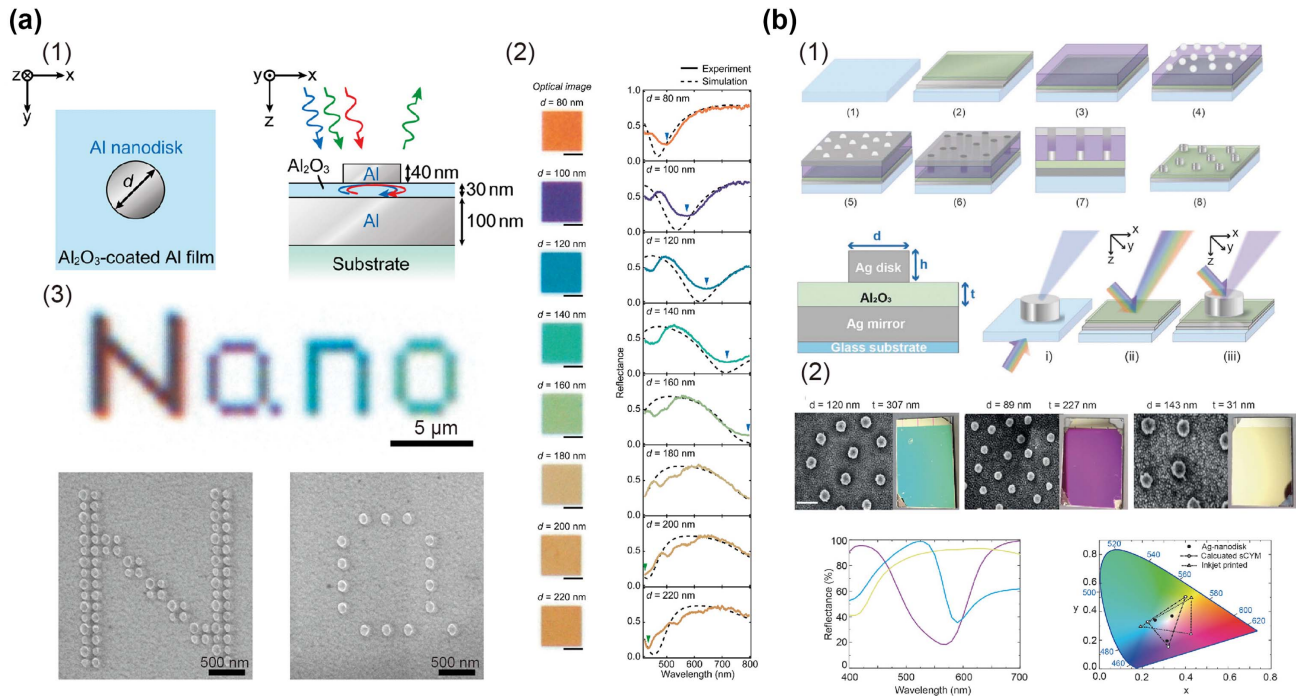


Fig. 6 Designs based on plasmonic resonances in the gap plasmon. (a) Schematic of gap plasmonic structure based on aluminum nanorods (1), and achieving structural color pixels with a single nanostructure and black pixels by blending different nanostructures (2)^[113]. (b) Process flow and structural schematic of large-scale preparation of Ag nanorod gap plasmonic structures using colloid lithography, along with samples and characteristics in CMY mode—cyan, magenta, and yellow (2)^[114].

gratings^[115,116], holes^[117], nanopillars^[118], etc.^[119–122] enables the manipulation of light through plasmonic effects. Structural colors based on metal plasmons can exhibit unparalleled performance, such as extremely high spatial resolution, excellent color stability, and simplicity in fabrication processes. Despite challenges related to brightness and color range, recent breakthroughs have addressed some of these issues, showcasing the potential of metal-plasmon-based structural colors in various applications, from display technologies to advanced optical encryption systems.

2.2 Dielectric-Materials-Based structural color

Dielectric metasurfaces offer another method for generating highly saturated structural colors, but with much higher optical efficiency compared to their plasmonic counterparts^[14,123–125]. Dielectric materials inherently exhibit advantages over metals including high losses leading to broadened peak shapes and lower efficiency. However, dielectric materials cannot achieve the strong field localization of light that metallic nanostructures can, so dielectric nanostructures often require array-enhanced electromagnetic multilevel resonances, resulting in lower spatial resolution compared to metallic nanostructures.

Fundamentally, dielectric metasurfaces realize structural colors via Mie resonances, which depend on the geometric shape and size of particles^[126,127]. Multiple Mie resonances have been observed in various dielectric nanostructures, such as nanowires^[128,129], rings^[124,130], bricks^[131], cylinders^[123,132], and so on^[50,133,134]. The variety of available structures provides opportunities to modulate electric or magnetic resonances by designing

specific geometric parameters. Apart from structural design, the physical properties of the material itself also significantly impact structural design.

Silicon (Si), as the most mature semiconductor material, has found widespread application in metasurface structural coloring. Si offers advantages such as low cost, high reliability, and compatibility with existing optoelectronic devices^[60,135]. Importantly, due to silicon's high refractive index, it can effectively localize and manipulate the light field, leading to strong electromagnetic resonances when subwavelength-sized Si nanoparticles interact with visible light wavelengths. Therefore, Si nanostructures are well-suited for use as color filters to achieve structural colors with high purity and a wide color gamut. The results show that compared to metal-based structural colors, Si-based metasurfaces can achieve better color display effects^[136,137].

In 2020, Yang *et al.* designed a 100 nm thick single-crystal Si nanodisk structure on a sapphire substrate, as shown in Fig. 7(a)^[138]. To address background reflection and the wide resonance peak formed by Mie resonances, the authors introduced a refractive index matching layer to reduce the refractive index contrast at the air-substrate interface, effectively reducing background reflection and suppressing wide resonance modes. As shown in Fig. 7(a) (2), with the introduction of dimethyl sulfoxide (DMSO) as the refractive index matching layer, background reflection was significantly suppressed, simultaneously effectively inhibiting wide resonance modes and improving color monochromaticity. From the CIE chromaticity diagram plotted in Fig. 7(a) (3), it is clear that with the introduction of DMSO as the refractive index matching layer, the color gamut area expanded to 135.6% of Adobe RGB. Due to the high

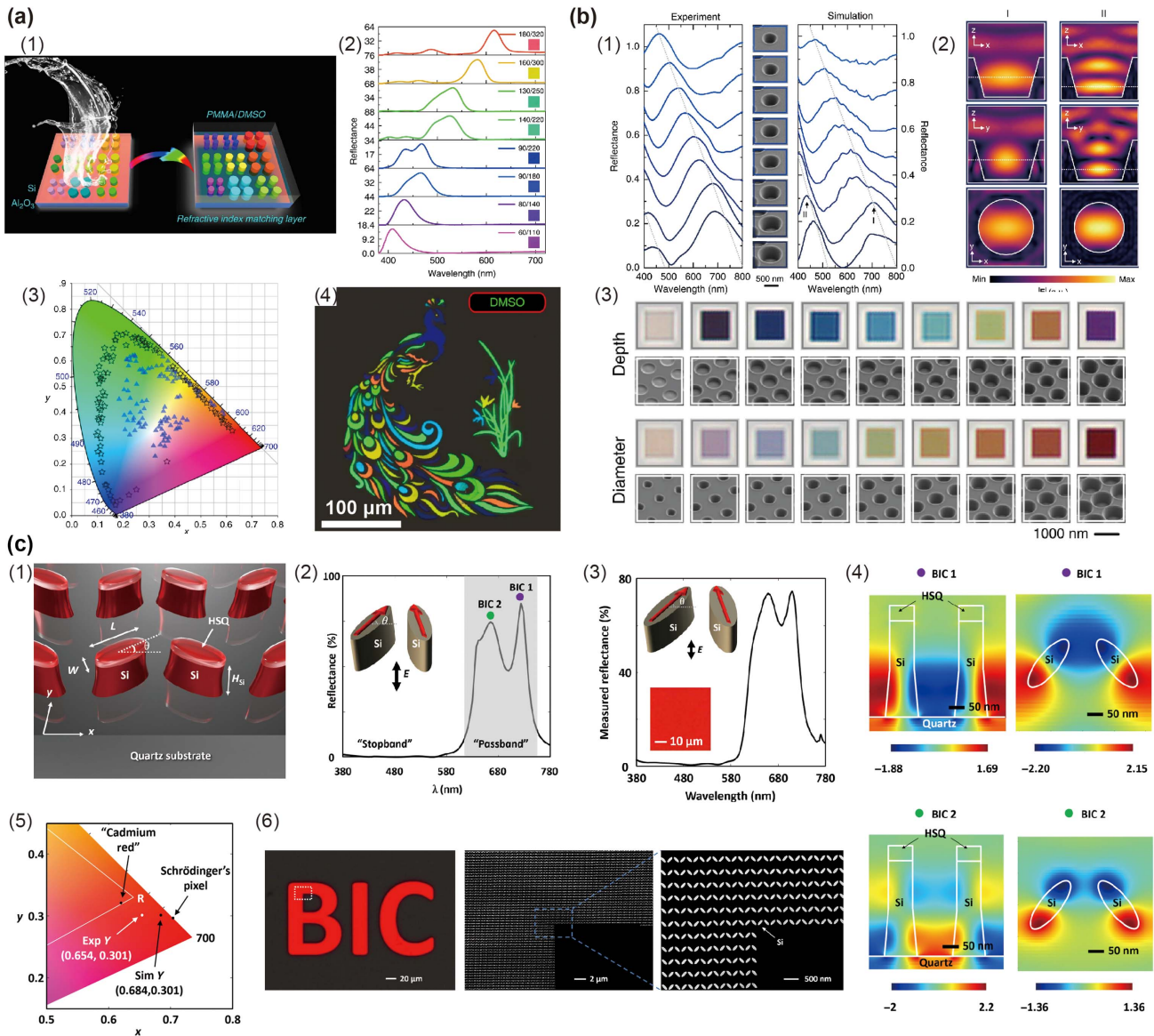


Fig. 7 Structural color design based on Si. (a) Si nanorod array on a sapphire substrate, introducing PMMA and DMSO as refractive index matching layers for high-performance structural color (1), reflection spectra, and CIE coordinates of the sample (2), (3), displaying a vivid phoenix pattern (4)^[138]. (b) Preparation of different-sized air holes on Si surface, localizing the electric field in the air, achieving Mie resonance structural color at short wavelengths, with reflection spectra and electric field decomposition as hole size varies (1)–(3)^[139]. (c) Schematic of high-saturation red design based on Si nanoantenna array BIC mode (1), simulation and actual reflection spectra, and corresponding CIE coordinates (2), (3), (5), E_z electric field components for both modes (4), and SEM image of the actual sample (6)^[140].

refractive index of single crystal Si, color display can be achieved with just a 2×2 nanodisk array, allowing the final spatial resolution to exceed 100,000 PPI. This design achieves high reflectivity, narrow half height and width (FWHM), large color gamut area, extremely high spatial resolution, and a simple preparation process, taking a crucial step towards the practical application of dielectric structural colors.

Due to the inherent strong absorption of Si at short wavelengths, which is unavoidable, and to address both the issue of absorption and material dispersion, Mario and colleagues proposed a strategy to confine light in subwavelength-sized

air cavities^[139]. They successfully achieved Mie resonances based on a Si substrate, even in the blue and ultraviolet range. To demonstrate the nature of the resonance modes, the electric field distribution at the resonant wavelength is shown in Fig. 7(b) (2), revealing the presence of electric dipole and magnetic dipole modes within the air voids. By adjusting the pore diameter on the Si substrate from 300 to 750 nm and the depth from 20 to 1100 nm, nanoscale color printing covering the entire visible spectrum was achieved. The reflection spectra and optical microscope images are illustrated in Figs. 7(b) (1) and (3).

Despite significant progress in structural colors based on Mie resonances, achieving highly saturated red remained a challenge. High-saturation red requires fundamental resonances wavelength beyond 600 nm, but Mie resonances supporting red fundamental modes often also support high-order modes in the blue range (380 to 480 nm). This results in a shift towards blue, appearing as degraded magenta or purplish-red colors. To address this issue, Dong *et al.* introduced quasi-bound states in the continuum (quasi-BIC) modes as reflection modes for modulation in the field of structural colors^[140]. They supported two partially overlapping quasi-BIC modes on a Si nanoantenna array, simultaneously suppressing high-order modes in the blue/green range through the design of diffraction channels induced by the substrate and the absorption of amorphous Si. This achieved a highly saturated red structural color. The designed amorphous Si nanoantenna was optimized using a gradient optimization algorithm with structural parameters $L = 235$ nm, $W = 85$ nm, $\theta = 47.9^\circ$, $\Delta x = 436$ nm, $\Delta y = 432$ nm, $H_{Si} = 360$ nm, as shown in Fig. 7(c). The simulated reflection spectrum in Fig. 7(c) (2) demonstrates distinct passbands and stopbands using quasi-BIC modes, closely resembling the spectrum required for an ideal Schrödinger red pixel. The actual measured reflection spectrum in Fig. 7(c) (3) aligns well with the simulation results. The CIE coordinates of the simulated and measured spectra are depicted in Fig. 7(c) (5). To verify the essence of the two response modes in the spectrum, Fig. 7(c) (4) shows the spatial distribution of E_z at the corresponding wavelength of the reflection peaks. Optical microscope and SEM images of the actual sample are presented in Fig. 7(c) (6).

While Si has a high refractive index, its unavoidable absorption losses at short wavelengths result in low efficiency and reduced saturation due to the broadening of the bandwidth in visible range. To address the optical characteristics of the material itself, researchers have turned to dielectric materials

with negligible losses in the visible light range, such as titanium dioxide (TiO_2)^[141–143], silicon nitride (Si_3N_4)^[144–146], and so on^[51,147,148]. Among these, TiO_2 , with its excellent optical properties and compatibility with CMOS processes, has found extensive use in the field of optics^[149–151]. The efficiency and sharp resonance of TiO_2 nanostructures supporting Mie resonances lead to high color saturation, easily surpassing the sRGB color gamut. However, due to the lower refractive index of TiO_2 compared to Si, larger structural units and larger periodic arrays are required to enhance Mie resonances. In recent years, significant progress has been made in the study of metasurface structural colors based on TiO_2 .

Sun and collaborators demonstrated a Mie resonance structural color design based on an array of TiO_2 nanoblocks^[134]. Figure 8(a) (1) shows a schematic of the proposed device, consisting of a trapezoidal-shaped array of TiO_2 blocks on a glass substrate coated with 15 nm indium tin oxide (ITO). And the trapezoidal angles are approximately 72° . The manufacturing technique for this structure is achieved through a simple lift-off process. The fabricated structure closely matches the design dimensions, as shown in Fig. 8(a) (2). The simulated and measured reflection spectra in Fig. 8(a) (3) achieve high reflectivity of over 64% and FWHM of approximately 30 nm. However, when the fundamental mode resonance wavelength is in the longer wavelength range (580 nm), high-order resonance modes gradually appear in the blue range, leading to a decrease in color saturation. The CIE coordinates of sample colors with low color saturation obtained from the experiment are shown in Fig. 8(a) (4). This is due to the decrease in monochromaticity caused by higher-order modes and Mie multipole resonance at short wavelengths, resulting in an unsatisfactory final color display effect.

To address the impact of high-order Mie resonance modes and Mie multipole resonance, Yang *et al.* designed a metasurface structural color using a multilayer dielectric stack to

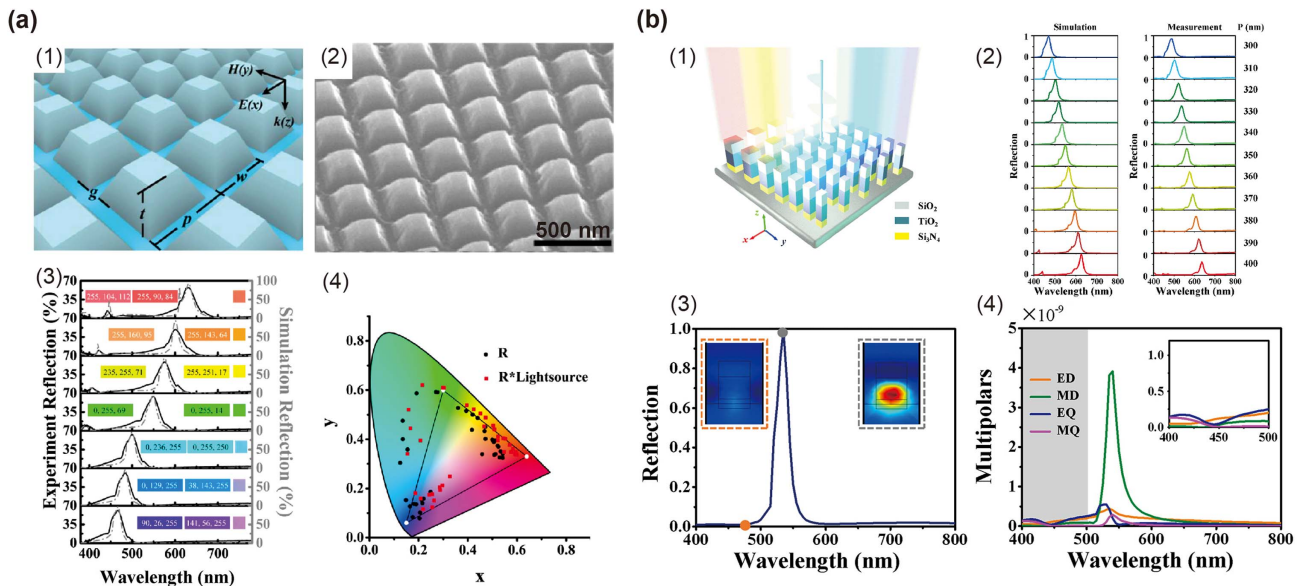


Fig. 8 Structural color design based on TiO_2 . (a) Design of trapezoidal TiO_2 nanorod array structural color (1), (2), reflection spectra, and CIE coordinates for different sizes (3), (4)^[134]. (b) Schematic of structural color based on multi-layer dielectric nanorods (1), reflection spectra covering the entire color space (2), and Mie decomposition for any structure proving suppression of high-order modes by multi-layer dielectric structures (3), (4)^[152].

achieve deep modulation of Mie multipolar resonance modes, significantly enhancing the monochromaticity of the reflected spectrum^[152]. As shown in Fig. 8(b) (1), the designed metasurface structure consists of an array of nanoblocks on a Si substrate. Each nanoblock structure, from top to bottom, is composed of vertically stacked layers of a 100 nm thick silica capping layer, a 140 nm thick TiO₂ spacer layer, and a 60 nm thick Si₃N₄ layer. The index matching between the SiO₂ layer between TiO₂ and air, and the Si₃N₄ layer between the silica substrate and the TiO₂ layer, significantly suppresses the short-wavelength multipolar modes, as shown in Fig. 8(b) (3). Due to the deep modulation of multipolar modes, as shown in Fig. 8(b) (2), varying the structural parameters allows for achieving high reflectivity, high spatial resolution, low FWHM, and high saturation in a full color structural color.

Dielectric-metasurface-based structural colors represent a cutting-edge approach to coloration technology. By harnessing the unique properties of dielectric materials, researchers have developed metasurfaces with nanostructured patterns that manipulate light to create vivid and customizable colors. Compared with metal plasmon, dielectric metasurface structural colors offer superior brightness, a narrower resonant mode, and enhanced stability. Although dielectric materials tend to have lower resolution, dielectric metasurfaces are expected to drive the application of structural colors in various fields with their excellent properties.

3 Advanced Design Methods

As meta-integration becomes more sophisticated and demands for increased functionality rise, forward design based on electromagnetic principles struggles to meet these challenges. Inverse design, on the other hand, aims to leverage mathematical tools to solve complex physical problems. In the early stages of research, various optimization algorithms such as evolutionary algorithms^[153,154] and topology optimization^[155] were introduced for the inverse design of complex metasurfaces^[156]. These approaches were widely applied in areas like multifunctional integration and 3D holography^[157,158].

When designing structural colors based on metasurfaces, the achievement of optimal color effects often requires the design and optimization of numerous parameters. These parameters include the shape, height, periodicity, and material of nanostructures and their optimization process can be time-consuming and computationally intensive. As research on structural colors deepens, traditional forward design struggles to achieve complex functionalities such as extreme color displays and multifunctional integration. Inverse design, utilizing mathematical tools, has become instrumental in addressing these challenges. In the early stages of research, various optimization algorithms, combined with electromagnetic simulation methods like rigorous coupled-wave analysis (RCWA) and finite difference time domain (FDTD), were used for the inverse design of structural color metasurfaces. However, design schemes based on methods like topology optimization and genetic algorithms often require substantial computational resources, escalating dramatically with increasing structural complexity.

With the advent of machine learning (ML), researchers have recognized its unprecedented capabilities for rapid solutions to multidimensional complex problems^[159]. However, ML, when used solely as a mathematical approach, may lead to physically unrealizable designs, significantly reducing design feasibility. In order to achieve efficient inverse design based on ML,

researchers have proposed physics-based deep neural networks to facilitate a more accurate spectral-structure inverse design process^[160–163].

In order to achieve more extreme control over electromagnetic waves on metasurfaces, there have been many recent studies that introduce optimization algorithms and ML into the design of metasurfaces^[154,164–170]. Additionally, color itself is the perception of electromagnetic waves by the human visual system, where different spectra could be perceived as the same color. Therefore, the ML approach is well-suited for the design of metasurfaces with structural colors to explore the feature relationships between spectra and human visual perception. Through ML-assisted design of metasurfaces, the time and computational power needed for structural design are significantly reduced, with the potential to achieve more saturated and vibrant color displays.

Pablo *et al.* proposed an open-source software package called Neural Inverse Design of Nanostructures (NIDN) that allows the designing complex, stacked material nanostructures using a physics base, which employs neural networks for structural design^[171]. Spectral calculations are carried out through integrated RCWA or FDTD algorithms, followed by optimization using backpropagation of errors, as illustrated in Fig. 9(a). A design that combines DNN modeling with simulation computation will greatly reduce the time and arithmetic requirements needed for metasurface design, and such a design provides a direction for future metasurface design.

Rho *et al.* employed a reinforcement learning model (Double Deep Q-Network, DDQN) to optimize the design of an all-dielectric structural color based on specific Si^[172]. Within the DDQN model, two similar models exist, with one serving as the main model and the other used to train the target model. Both models contribute weights during training. The training process involves the DDQN providing geometric data, creating simulation models, obtaining color information based on reflection data, calculating a loss function according to color, and performing parameter optimization for the next iteration. As shown in Fig. 9(b) (1), DDQN was used to design the diameter, period, and layer thickness of Si nanodisks on an antireflection Si₃N₄ film on a Si substrate, achieving more saturated structural colors compared to non-DDQN designs, as depicted in Fig. 9(b) (2)^[132].

While Rho introduced ML to achieve better color saturation, significant time still needs to be invested in simulation calculations, which may not be conducive to high-speed spectrum-guided structural design. Elsayy *et al.* employed a deep-learning-driven inverse design approach for a structural color metasurface, whose design process is illuminated in Fig. 9(c) (1)^[173]. This method combines a multi-valued artificial neural network (MVANN) with backpropagation optimization, achieving spectral optimization for a four-parameter structure with only 585 training data points. The trained MVANN model demonstrated the ability to predict the spectrum of geometric structures beyond the training dataset, showcasing reliable predictions even with a limited training set. The inverse design further allowed the construction of geometric structures based on the predicted spectrum. The model was scanned across the visible light spectrum, covering the entire spectrum, and the predicted spectrum was compared to the simulated spectrum. The resulting CIE coordinates and reflection spectra are illustrated in Figs. 9(c) (2) and 9(c) (3).

In summary, the incorporation of algorithms, ML, and other captivating design tools is expected to significantly accelerate

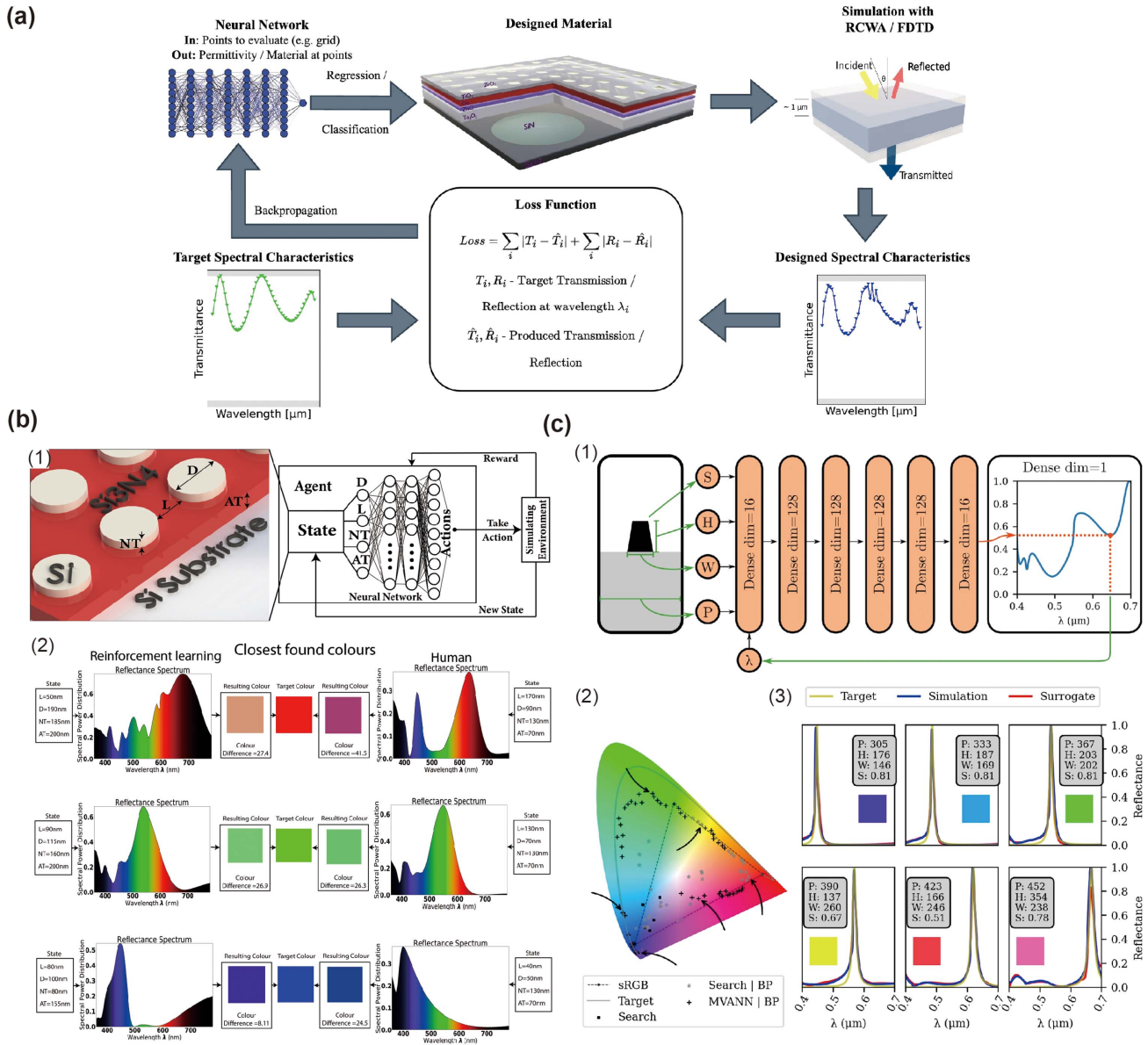


Fig. 9 Design of metasurfaces using DNN. (a) General flowchart of metasurface design using DNN^[171]. (b) Reinforcement learning is applied to the design of an all-dielectric structural color. The structure model based on Si and the training process (1); ML training results achieve higher color saturation compared to previous human-designed structures (2)^[172]. (c) Training and spectral prediction of TiO₂ grating structure using MVANN. Training model and training process for the four parameters of the structure and their corresponding spectra (1). (2) Color gamut distribution after network optimization, where arrows indicate the colors corresponding to the spectra in (3)^[173].

the development of the structural color field. Additionally, the use of ML holds the promise of exploring higher-dimensional latent correlations between spectra and the human visual system. Numerous studies have already trained DNN models to achieve inverse designs of colors and spectra. However, the training of DNN requires a substantial amount of accurate and effective data, making the widespread application of DNN in metasurface design more challenging.

4 Dynamic Tunable Structural Colors

As numerous researchers delve into the geometric shapes, material properties, and spatial arrangements of micro-

nanostructures on metasurfaces, an increasing number of high-performance structural colors are being designed. However, traditional metasurfaces, once fabricated, lack adjustability, making them unsuitable for the dynamic tuning demands of most devices. Consequently, dynamic tunable structural color displays have become an urgent necessity. In recent years, various materials and optical mechanisms have been employed to achieve dynamically tunable metasurfaces^[174].

Dynamic tunable structural colors hold the potential to be integrated into next-generation displays, offering reduced power consumption, enhanced readability, and resolution improvement, especially in wearable displays. Reflective displays differ

from emissive/backlit displays (LCDs, LEDs, and OLEDs) in their utilization of ambient light, resulting in significantly lower power consumption. Emitting/backlit displays are often the most power-consuming components in portable devices. One advantage of reflective displays is their ability to use bright external light sources to illuminate display components. Achieving high brightness is a challenge for micro displays, and high-resolution reflective displays based on tunable structural colors can play a crucial role in portable devices.

Fundamentally, achieving dynamically tunable structural colors on metasurfaces involves two main approaches: switching active materials to different states and geometric reconstruction of the metasurface. For active materials, control of the material refractive index can be achieved through external stimuli such as lasers^[179,180], thermochromic^[181,182], voltage^[183–190], magnetic control^[191–195], and chemical reactions^[196,197]. Voltage-driven control of internal components of the material through ion driving is an effective means of dynamic control. Recent research has utilized Si nanostructures as electrodes in lithium-ion batteries, achieving dynamic structural colors driven by voltage, as shown in Fig. 10(a)^[175]. Figure 10(b) illustrates that dynamic structural colors based on reversible chemical processes are considered a

feasible approach^[176]. Reversible hydrogenation processes involving materials like Mg and TiO₂ can strongly alter the optical properties of materials^[176,197], enabling resonance tuning. Additionally, dynamic structural colors controlled by external factors such as laser pulses and magnetic fields are widely studied^[193,194,198]. Notably, dynamic tuning based on phase change materials is particularly promising, given the significant refractive index changes during phase transitions that can easily achieve color control.

Many researchers have also explored the reconfiguration of metasurfaces to achieve dynamic adjustments of structural colors. The optical response responsible for structural colors, such as SPR and Mie resonance, is highly sensitive to the shape and periodicity of metasurface units. Reconfiguring the metasurface allows control over the entire system's optical response. By introducing microfluidic systems and adjusting the refractive index of the environment^[177,199,200], control over resonance wavelength can be achieved, as depicted in the dynamic structural color model based on a microfluidic system in Fig. 10(c)^[177]. Additionally, unique designs for metasurfaces enable differential color responses to different states of the incident light field, allowing for rapid color switching by adjusting the incident light

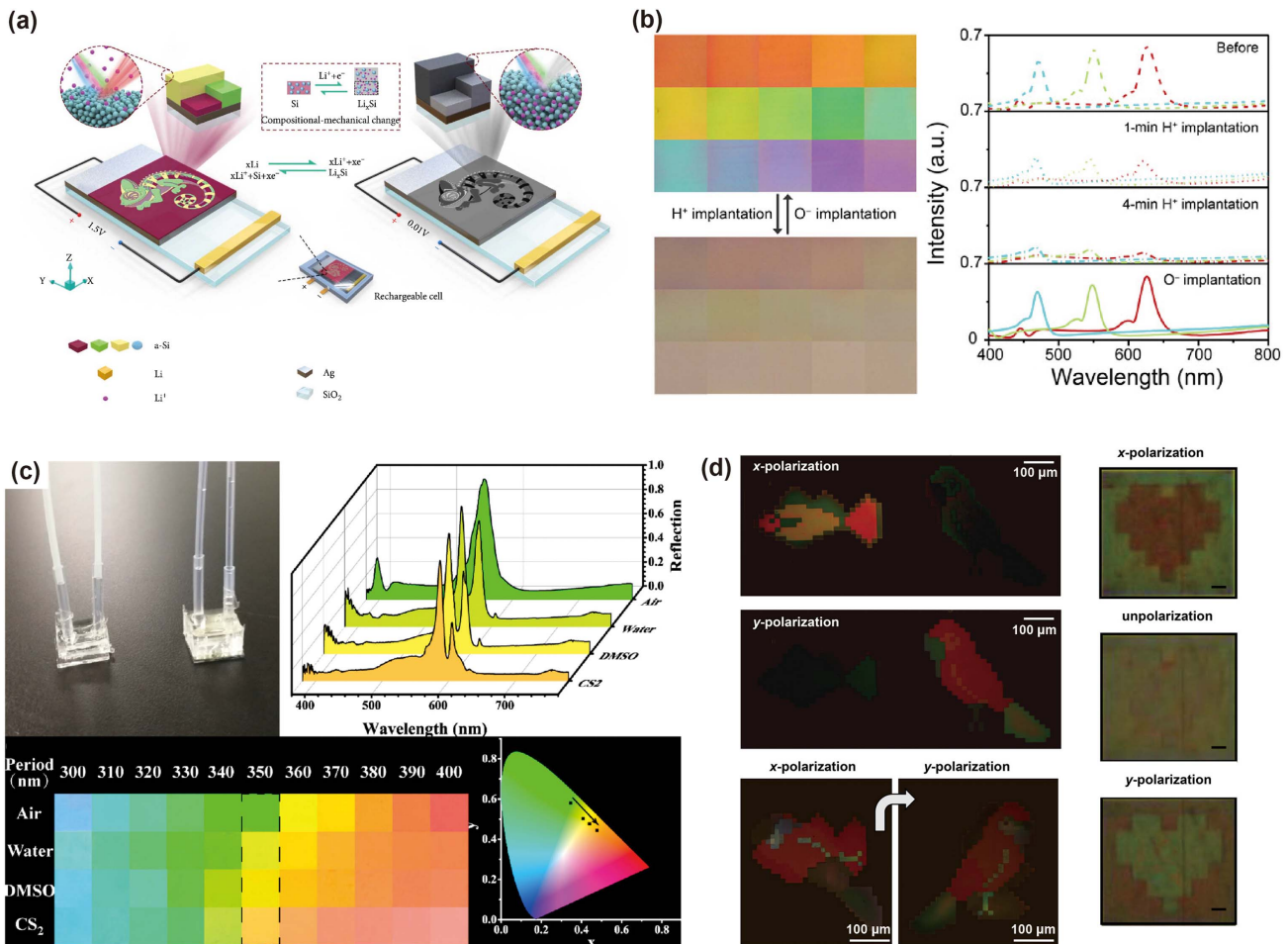


Fig. 10 Various design methods for achieving dynamic structural colors are illustrated. (a) Dynamic structural color achieved through voltage-driven ion injection^[175]. (b) Erasable structural color based on a reversible hydrogenation-oxidation process^[176]. (c) Dynamic structural color achieved through microfluidic control^[177]. (d) Brightness-changing structural color based on polarization^[178].

state^[201–204], as shown in Fig. 10(d)^[178]. The simplest and most practical method is to induce mechanical strain to alter the arrangement of the metasurface, achievable through MEMS systems or flexible substrates^[205–208].

4.1 Phase Change Material

The addition of phase change materials to metasurfaces allows for reversible switching between different spectral responses through external stimuli. Vanadium dioxide (VO_2) has garnered attention due to its excellent thermal stability and reversible insulator-metal transition (IMT). In comparison to other materials, VO_2 exhibits a relatively low IMT transition temperature ($T = 68^\circ\text{C}$) and faster transition speed (picosecond level)^[209,210], which has been used as thermochromic smart windows^[211]. He *et al.* designed a fully visible band switchable dynamically tunable absorber (DTA) based on VO_2 , with the proposed MIM structure shown in Fig. 11(a) (1)^[212]. The structure consists of a top layer of periodically perforated Ag, an intermediate layer of VO_2 , and a bottom layer of silver. By controlling the temperature of DTA to modulate the VO_2 phase transition, a significant switching function is achieved across the entire visible light spectrum, as illustrated in Fig. 11(a) (2). This absorption change results in a noticeable color variation, depicted in Fig. 11(a) (3), showcasing the color change before and after the VO_2 phase transition.

While VO_2 exhibits excellent phase change performance, its phase transition process is volatile, hindering the preservation of color information in different states. $\text{Ge}_2\text{Sb}_2\text{Te}_5$ (GST), as a mature phase change storage material, benefits from its significant optical performance change between crystalline and amorphous states. Its polymorphic adjustability allows for multilevel

information storage^[213,214]. As early as 2014, research groups attempted to achieve dynamically tunable structural colors using GST material. In a study by Hosseini *et al.*, a reflective display based on GST film was designed^[215]. The GST film is sandwiched between two layers of transparent ITO electrodes and deposited on the surface of a metal reflector, as shown in Fig. 11(b) (1). Color control is achieved by adjusting the thickness of each film layer, as illustrated in Fig. 11(b) (3). The GST pixels are pixelated, enabling an electrically switchable display where each pixel can be randomly accessed and manipulated, as depicted in Fig. 11(b) (2). By replacing the metal reflector on the back of the film with a transparent substrate, a semi-transparent display based on PCM can be realized. The structure is optimized from top to bottom with 20 nm thick ITO, 7 nm thick GST, and 40 nm thick ITO layers. Due to the thin thickness of the film, it can be deposited on flexible substrates, enabling a low power, ultrathin flexible display, as shown in Fig. 11(b) (4). Integrating PCM as an active switch for structural colors into the display makes ultrathin, low-power flexible displays possible.

However, GST's relatively high optical losses in the visible light range make it challenging to achieve high-brightness structural colors. Another emerging PCM, antimony sulfide (Sb_2S_3), has gained widespread attention due to its intense optical property changes, polymorphic adjustability during phase transitions, and lower optical losses in the visible light spectrum^[216]. Lu *et al.* utilized Sb_2S_3 to design a triple-resonance reversible and tunable dielectric nanodisk array, achieving nonvolatile, high-speed, and reversible tuning of Mie-resonance-based structural color devices^[217]. The Sb_2S_3 and Pd multilayered nanodisk array, arranged on a 200 nm thick SiO_2 film on a Si substrate, is shown in Fig. 12(a) (1). The Pd layer, serving as the etching

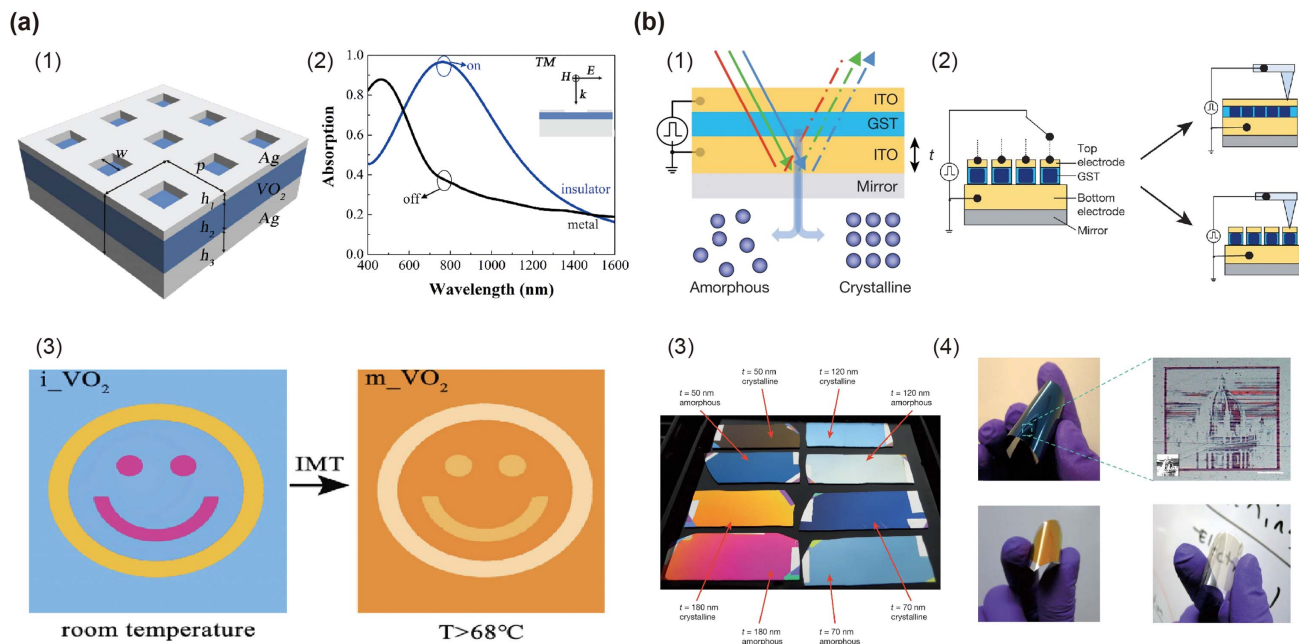


Fig. 11 Dynamic structural color design based on VO_2 and GST phase change materials. (a) VO_2 as a tunable dielectric spacer in MIM structure (1), and absorption and color changes before and after phase transition (2), (3)^[212]. (b) Dynamic structural color design based on GST, schematic of dynamic film and pixel tunable display structure (1), (2), structural colors with different film thicknesses (3), and schematic of flexible transparent display sample (4)^[215].

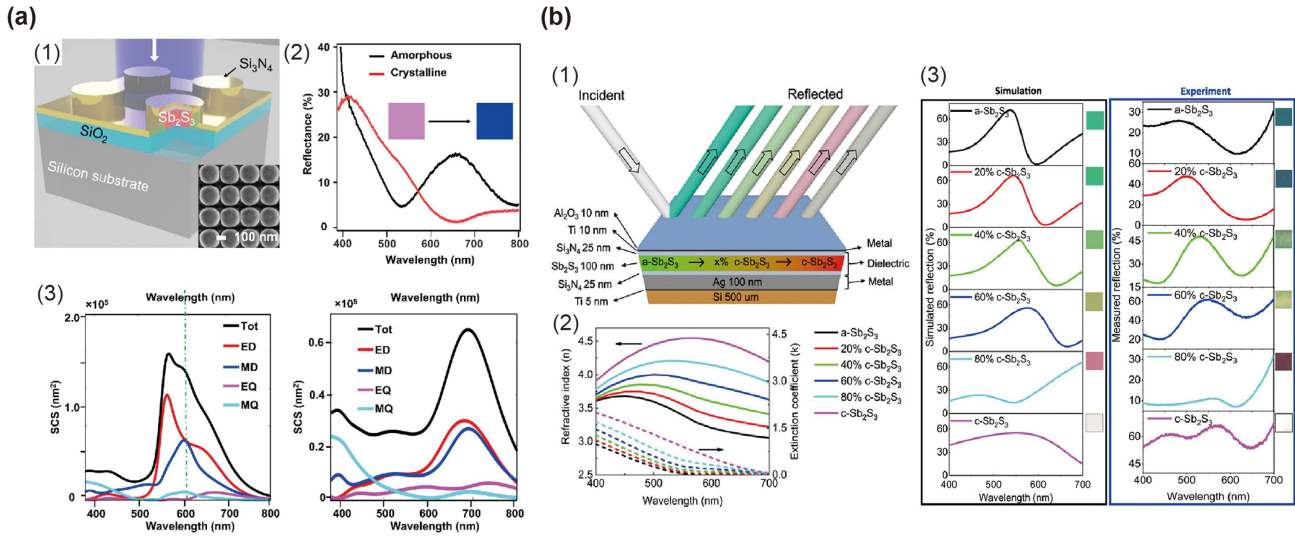


Fig. 12 Dynamic structural color design based on Sb_2S_3 . (a) Mie resonance structural model based on Sb_2S_3 nanorods (1), reflection spectra changes before and after phase transition (2), and Mie decomposition (3)^[217]. (b) Dynamic tunable FP resonance mode based on Sb_2S_3 (1), continuous color change achieved by controlling intermediate states of Sb_2S_3 phase transition, enabling multilevel adjustment of refractive index (2), (3)^[218].

mask for Sb_2S_3 during inductively coupled plasma (ICP) etching, is deposited. Subsequently, a 70 nm Si_3N_4 layer is deposited to act as an anti-reflection coating, preventing the loss of sulfur (S) atoms during the phase transition process. Control over the Sb_2S_3 phase transition is achieved using a 780 nm, 80 MHz, 100 fs laser pulse, enabling a scanning speed of 10 $\mu\text{m/s}$ at a power of 12 mW. The drastic refractive index change between the crystalline and amorphous states induces significant variations in the resonance modes, as observed in the reflection spectra in Fig. 12(a) (2). The multipole decomposition of the scattering cross-section is presented in Fig. 12(a) (3), illustrating the dynamic switching of structural colors as the Sb_2S_3 nanodisk transitions from the amorphous to crystalline state due to changes in the interaction between electric and magnetic dipole resonances.

Additionally, Omar *et al.* designed an all-optical switching structural color device based on Sb_2S_3 ^[218]. Figure 12(b) (1) illustrates the schematic of a multilayer film structure, where a 5 nm titanium (Ti) layer is first deposited to enhance the adhesion of Ag, followed by a 100 nm thick Ag layer serving as the back reflector. The dielectric portion consists of two layers of 25 nm thick Si_3N_4 (to separate the metal layer from the Sb_2S_3 layer) sandwiching a 100 nm thick layer of Sb_2S_3 . Subsequently, a 10 nm Ti layer and a final protective layer of 10 nm Al_2O_3 are deposited. Control over multiple intermediate states of incomplete phase transition in Sb_2S_3 is achieved by controlling the continuous wave (CW) laser pulse density from 0 to 200 kW/cm^2 at a constant laser scan speed of 20 $\mu\text{m/s}$, enabling switching between various refractive index states, as shown in Fig. 12(b) (2). Experimental validation demonstrates the multifunctionality of achieving various structural colors using the phase transition intermediate states in a single-layer Sb_2S_3 film within the MDM cavity. The transition from amorphous to fully crystalline state results in a resonance wavelength change of 220 nm, producing colors from green to red, as depicted in Fig. 12(b) (3).

4.2 Liquid Crystal with Polarization Sensitive Metasurface

Unlike the phase change materials discussed earlier, which control optical responses by altering the material's refractive index, the design of polarization-sensitive meta-atoms enables polarization-dependent optical responses. This approach allows color switching without changing the geometric shape or material composition. Numerous studies have explored polarization-dependent structural colors for applications such as dynamic color displays, high-density optical information storage, optical encryption, and multi-channel imaging^[51,178,219,220].

Due to the optical anisotropy of liquid crystals (LCs), they exhibit different refractive indices in different directions, resulting in phase delays along different directions. Through the specific design of LCs, their ability to control polarization can be utilized. For instance, widely used LCDs rely on the control of polarization achieved by LCs. Recently, the development of tunable metasurfaces by combining LCs with metasurfaces has attracted much interest. For instance, researchers have integrated LCs with metasurfaces to create a device capable of dynamically displaying colors through voltage-controlled LC polarization modulation^[221]. In terms of commercial applications, liquid crystals are well-established commercial optical materials that have been extensively studied by many companies for the design of commercially available tunable metasurfaces, and exciting results have been achieved at telecommunication wavelengths^[222,223]. However, the combination of LCs and metasurfaces has not yet been successfully applied in commercial products for tuning structural color and remains in the laboratory stage.

Li *et al.* integrated a polarization-dependent plasmonic metasurface with a polymer-dispersed liquid crystal (PDLC) as a polarization analyzer, achieving further encryption of transmitted light^[224]. The operational schematic of the device is depicted in Fig. 13(a) (1). By designing Al nanoapertures with different responses to x and y polarizations, the metasurface selectively

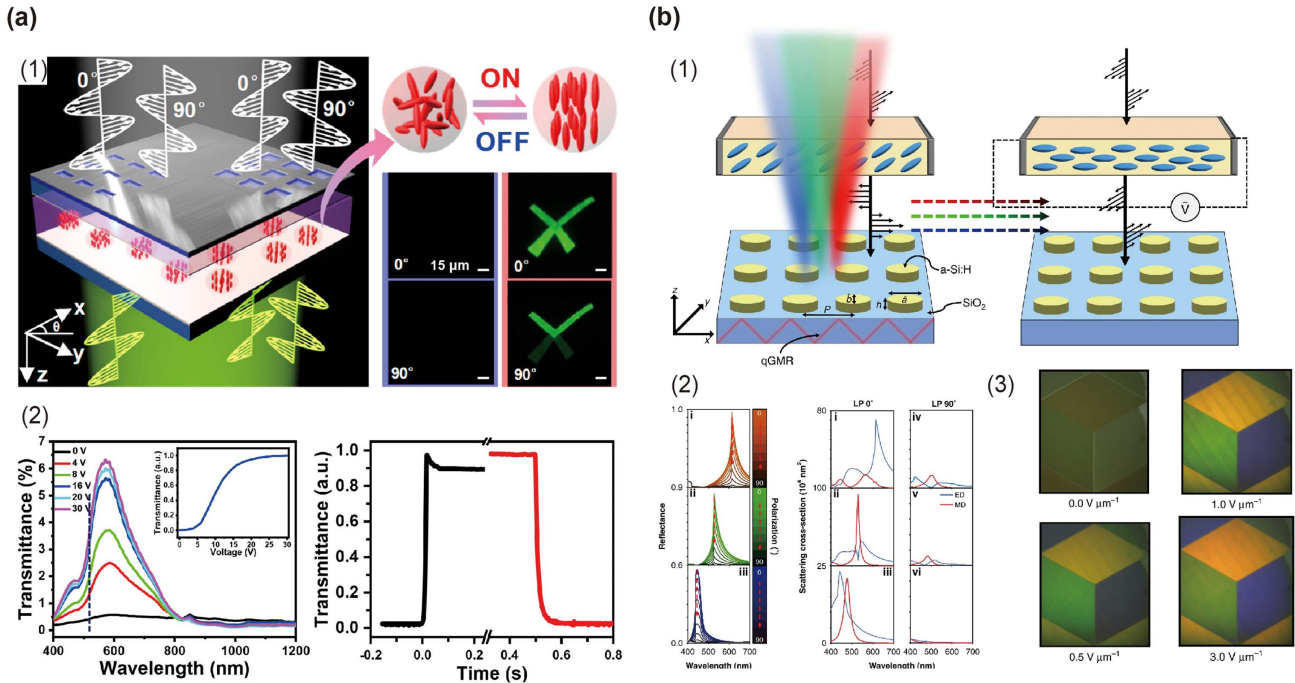


Fig. 13 Dynamic structural color adjustment using liquid crystal and polarization-sensitive metasurfaces. (a) Anisotropic Al nanoholes integrated with LC for switchable structural color display (1), and voltage-induced modulation of transmission intensity with a switch time on the order of milliseconds (2)^[224]. (b) Elliptical Mie resonators integrated with LC for brightness-adjustable dynamic color display (1), continuous changes in RGB color brightness under different polarizations (2), and dynamic color display of actual samples with increasing voltage (3)^[225].

displays images corresponding to specific polarization responses. Dynamic control of transmittance is achieved by applying voltage to the liquid crystal, with response and recovery times of 8.7 and 29.8 ms, respectively, under a 17 V voltage, as illustrated in Fig. 13(a) (2).

Rho's research team opted to integrate LC as a polarization generator with polarization-sensitive Mie resonators to achieve brightness-adjustable reflective structural colors, as illustrated in Fig. 13(b) (1)^[225]. The proposed Mie resonators consist of hydrogenated amorphous silicon (a-Si:H) ellipsoidal cylinders, arranged in a lattice with a specific periodicity. The desired spectral response is generated through the hybridization of Mie scattering with the periodic array's quasi-guided mode resonance (qGMR). The spectral variations of the designed RGB primary colors with changing polarization are shown in Fig. 13(b) (2). Subsequently, LC is integrated as a polarization generator on the metasurface, enabling brightness control of colored patterns through voltage modulation, as depicted in Fig. 13(b) (3). By combining and arranging meta-atoms with different color responses, mixed colors can be generated, and combinations of red, green, and blue can produce white. The design based on polarization-sensitive and liquid crystal elements can find applications in various fields, including advanced optical encryption, optical anti-counterfeiting, multi-channel imaging, and dynamic displays.

4.3 Mechanically Controlled structural color

Mechanically controlled metasurfaces were initially inspired by micro-electro-mechanical systems (MEMS), where temperature

and voltage can be used to control micro-scale mechanical systems, thereby influencing the optical response of the combined metasurface at a microscopic level^[226,227]. Aaron *et al.* designed a voltage-controlled MEMS combined with a metasurface capable of selecting or mixing specific colors^[228]. The proposed structure uses silicon-on-insulator (SOI) technology to suspend Mie resonators on a Si substrate, as shown in Fig. 14(a) (1). The metasurface, composed of Si nanobeams (cross-sectional size 100×100 nm), creates vibrant reflective structural colors through the coupling of Mie resonance and FP modes between the substrate and the metasurface. The driving capability of voltage for different thicknesses of Si metasurfaces was measured, as depicted in Fig. 14(a) (2). At a thickness of 100 nm, only 3 V of voltage was needed to drive over 100 nm displacement. By adjusting the voltage to control the height of the Mie resonator, dynamic tuning of the FP resonance wavelength was achieved, allowing the appearance of desired characters, as shown in Figs. 14(a) (3) and 14(a) (4).

While dynamic structural colors based on MEMS have achieved significant progress, the complex composition of MEMS structures and their integration with metasurfaces pose significant challenges in terms of processing and design, greatly limiting the effective application of structural color devices. However, stress-induced modulation based on a flexible substrate is a simple and effective control method. Zhang *et al.* investigated the dynamic tuning of TiO₂ metasurface structural colors through PDMS stretching, achieving polarization insensitivity in two independent mechanisms parallel and perpendicular to the stretching direction, as illustrated in Fig. 14(b) (1)^[229]. The metasurface is presented as an inverse

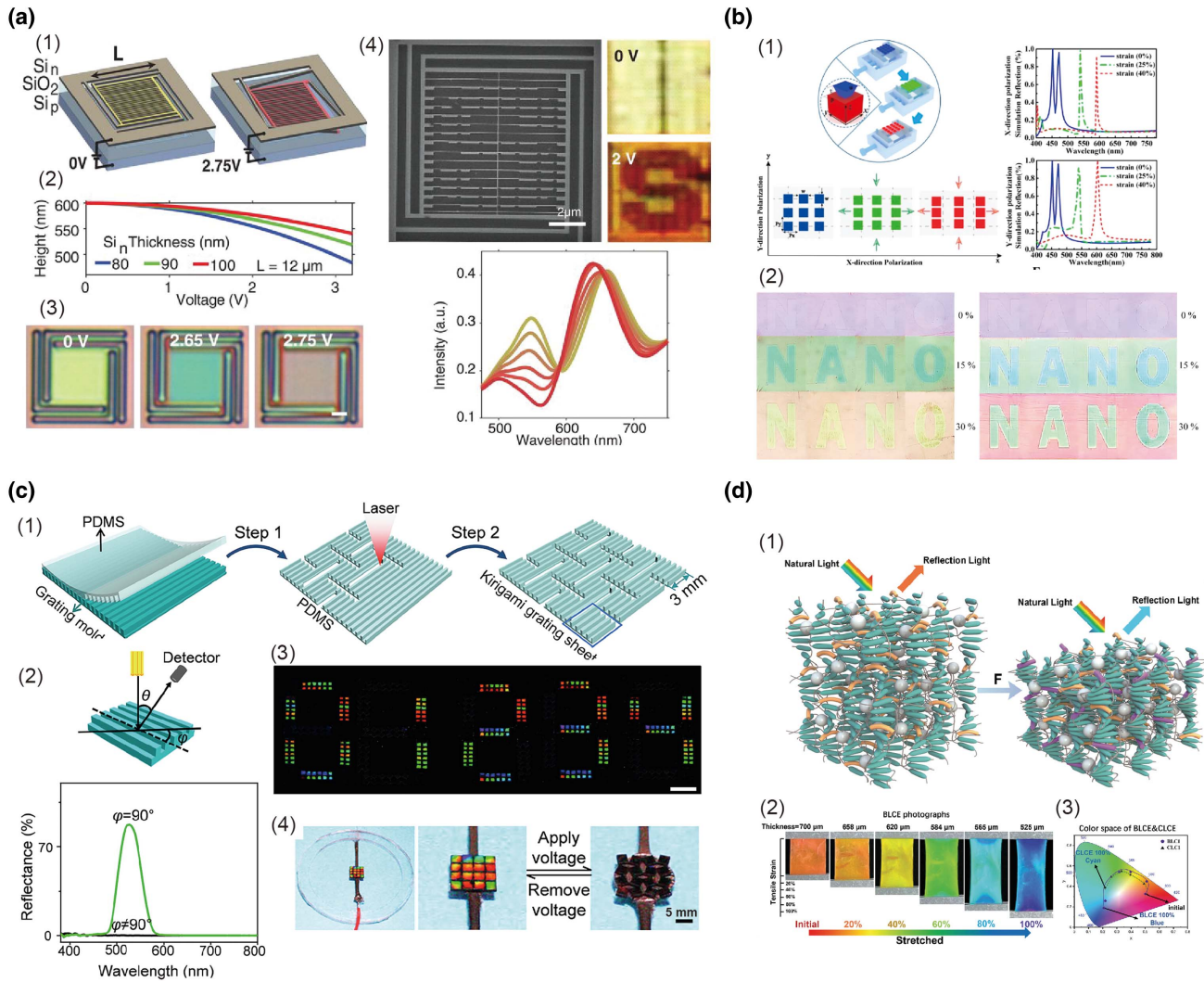


Fig. 14 Dynamic structural color based on mechanical stress-induced structural changes. (a) Voltage-tunable FP resonance mode, adjusting grating structure height with changing voltage (1), (2), lowering height to induce resonance wavelength changes, and achieving color changes (3), (4)^[228]. (b) TiO_2 nanostructure array prepared on a flexible substrate (1), and dynamic adjustment of structural color by applying external stress (2)^[229]. (c) Kirigami grating structure prepared via nanoimprinting and laser etching (1), grating structure exhibiting strong selectivity for observation angle (2), and dynamic structural color display achieved by applying external force or combining with a drive motor (3), (4)^[230]. (d) Composite of ATO nanoparticles and mechanically responsive color-changing pigment in a highly elastic liquid crystal substrate (1), achieving dynamic color changes with high saturation and a wide color gamut (2), (3)^[231].

trapezoidal TiO_2 nanostructure array embedded in a PDMS flexible substrate. Through the analysis of the scattering cross-section's multipole decomposition, clever adjustments to the structural parameters enable the movement of resonance positions based on deformation under different polarization states, allowing for information display and concealment, as shown in Fig. 14(b) (2).

Inspired by the structural color changes caused by the movement of animal feathers, Hou *et al.* designed a structure that utilizes topological spatial deformation on a two-dimensional (2D) plane with a kirigami structure to manipulate the direction of a 1D grating^[230]. The topological deformation generated by stretching allows for predictable and precise adjustment of

pixelated grating direction, enabling controlled changes in structural color. The gratings, made of PDMS flexible material, were mass-produced using nanoimprint technology, and pixelated gratings were cut using laser cutting, as shown in Fig. 14(c) (1). Figure 14(c) (2) demonstrates that vibrant structural colors can only be observed at an observation azimuth angle of 90° . The essential nature of topological deformation induced by external stress is changing the orientation of grating pixel blocks. Selective stretching of the kirigami grating can achieve independent control of each segment, as depicted in Fig. 14(c) (3). It can also be combined with a dielectric elastomer actuator drive to achieve voltage-driven dynamic structural colors, as shown in Fig. 14(c) (4).

In a different approach, inspired by the color-changing ability of cephalopod skin^[232], Sun and collaborators proposed a biomimetic liquid crystal elastomer film (BLCE) based on force-induced coordinated changes in pigment and structural colors^[231]. Control over mechanical sensitivity was achieved by adjusting the concentration of antimony-doped tin oxide (ATO) nanoparticles, as illustrated in Fig. 14(d) (1). When the critical elongation rate for the pigment is not reached, the color is primarily caused by the structural color resulting from changes in the spacing of the liquid crystal elastomer helix. After exceeding the critical elongation rate, the color exhibits a combined effect of structural and pigment colors, achieving continuous dynamic color changes from red to blue at elongation rates from 0% to 100%, as shown in Figs. 14(d) (2) and 14(d) (3). Combining force-induced pigments and structural colors, the design of BLCE film effectively addresses the issues of low elongation rate and small viewing angle of PDMS substrates. Due to its outstanding force-induced response and a sufficiently large color display range, BLCE films hold great potential in applications such as mechanical sensors and anti-counterfeiting materials.

5 Applications of structural color

In the preceding sections, we have explored numerous research achievements in static and dynamic structural colors. Thanks to the high-performance color display, stability, and resolution advantages of structural colors, those based on metasurfaces have found wide applications in various fields such as displays, optical encryption, structural color inks, colorimetry, sensing, and more^[189,190,233–235].

5.1 Display Technology

With pixel densities, brightness, and color saturation surpassing current displays by two orders of magnitude, structural colors are being recognized by numerous researchers as formidable contenders for the next generation of high-performance displays^[236,237]. Substantial research efforts have been dedicated to structural color displays to harness their superior capabilities. To achieve *in-situ* dynamically reconfigurable structural color displays, Yan *et al.* devised a floating solid thin film (FSTF), as illustrated in Fig. 15(a) (1)^[188]. The film, consisting of a 45 nm thick ITO layer, a 70 nm thick iron oxide layer, a 140 nm thick Ag layer, and a 100 nm thick TiW layer, undergoes reconfiguration by applying bias voltages to the ITO and TiW electrodes, thereby driving the movement of Ag ions. The cross-sectional SEM of the FSTF sample is depicted in Fig. 15(a) (2). Without bias, the resonant wavelength can be controlled by adjusting the thickness of the Fe_2O_3 layer, as shown in Fig. 15(a) (3). As illustrated in Fig. 15(a) (4), choosing a 70 nm Fe_2O_3 layer, and applying a 1 V positive bias to the electrode, results in a color transition from orange to purple, blue, and green over time. Reversing the process with a 1.3 V inverse bias enables reversible changes in structural color. Each color state is non-volatile, exhibiting long-term optical stability. Subsequently, flexible FSTF films were prepared on a flexible substrate, displaying a wide viewing angle and polarization insensitive characteristics, making them highly suitable for flexible display technologies.

Joo *et al.* designed a metasurface-based OLED display screen serving as a coordinated back reflector, achieving an ultra-high resolution of over 10,000 PPI^[238]. The structure of

the meta-OLED device is depicted in Fig. 15(b) (1), where an Ag nanopillar array is constructed on the Ag reflector, and OLED structures for RGB emitters and charge transport layers are built on the metasurface. Figure 15(b) (2) illustrates the color representation of nanopillars with different structural parameters, with the background color determined by the OLED layer's thickness. This outcome indicates that a judicious combination of OLED and metasurface allows for achieving any desired color in the visible spectrum. Due to the increased design flexibility provided by the metasurface for OLEDs, coupled with the Purcell effect, the meta-OLED exhibits superior emission performance and a shorter spectrum compared to color-filtered white OLEDs, as shown in Fig. 15(b) (3). Accurate color display and high brightness standards are maintained even at a sub-pixel size of 1.2 μm , achieving a pixel density of 10,000 PPI, as illustrated in Fig. 15(b) (4). The OLED design based on metasurface structural colors is poised to be a formidable contender for the next generation of micro displays, boasting high saturation, brightness, and exceptional spatial resolution, making it one of the most practical applications of metasurface structural colors.

Different from traditionally applying structural colors to 2D flat displays, Joel and colleagues employed a 3D display technology proposed by Nobel laureate Gabriel Lippmann^[239,240]. They combined structural color planes with a micro-lens system, achieving 3D structural color displays observable to the naked eye under diffused light, as illustrated in Fig. 15(c) (1)^[241]. To achieve a seamless integration of micro-lenses and structural colors, a two-photon polymerization 3D printing technique was employed to simultaneously print nanopillars and micro-lenses. The micro-lens had a curvature radius (R) of 22 μm and a diameter (L) of 21 μm . The positions of the micro-lenses and the arrangement of nanopillars were determined through ray-tracing calculations. The actual structure is depicted in Fig. 15(c) (2).

5.2 Optical Multi-Regulation

Due to the multidimensional control of light achieved by metasurfaces, unique responses to different states of light can be realized through the unique design of metasurface units^[242]. Exploiting this capability, structural colors find widespread applications in optical multi-states information regulation. Typically, utilizing the anisotropy of meta-atoms to achieve different colors for various polarization states is the most common optical encryption method^[243–247]. Alternatively, multiple colors can be further encoded using encryption techniques such as binary or Morse code^[186,248,249]. However, achieving foolproof advanced optical encryption with these methods can be challenging. To achieve a higher level of optical encryption, Joel's research group combines structural colors with OAM^[250]. By associating different orders of OAM with colors, optical information is stored in the form of OAM and color. The information is decrypted using a physical key, enhancing optical security. To improve the signal-to-noise ratio, they introduce a converging phase in the color-topological vortex beam (CVB). The actual CVB sample is depicted in Fig. 16(a) (1). Since color and topological charge are independent, a single CVB array can be used for multidimensional information storage and optical anti-counterfeiting, as shown in Fig. 16(a) (2). In a single CVB array, the color displays the information "SUTD," while the topological charge shows mathematical information, allowing independent control of any piece of information.

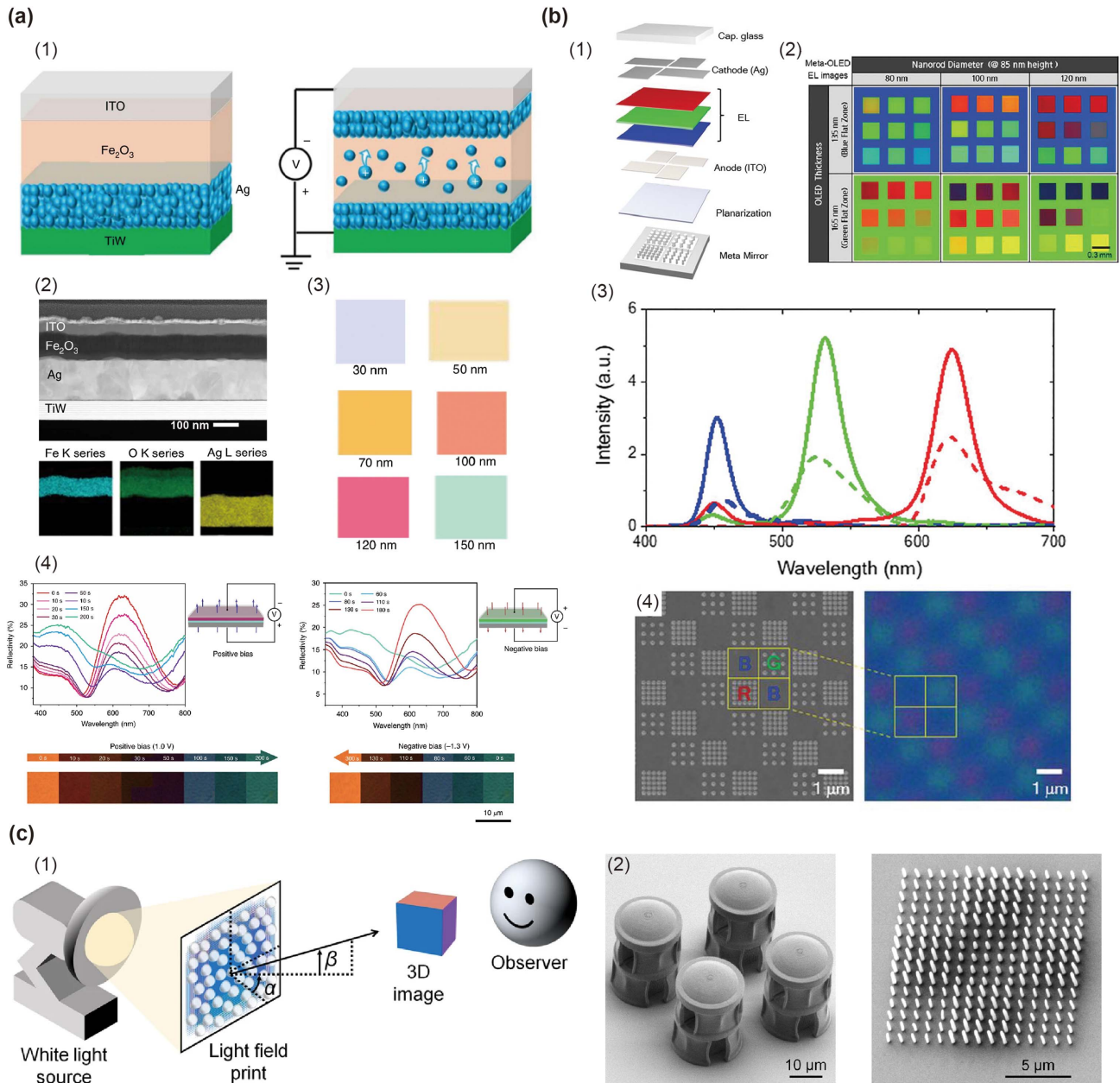


Fig. 15 Applications of structural color in the display. (a) Voltage-driven *in-situ* color-changing multilayer film structure (1), (2), initial colors of different thicknesses of Fe_2O_3 layers (3), and reversible color changes under positive and negative bias (4)^[188]. (b) High-resolution OLED design based on structural color surfaces (1), controlling FP mode by adjusting OLED layer thickness (2), achieving higher brightness at the same power due to reduced optical losses of traditional color filters, and maintaining good color display even with a minimum subpixel structure of $1.2 \mu\text{m}$ (3), (4)^[238]. (c) Combining color filters with micro lenses to achieve 3D structural color display is illustrated. Schematic diagram of 3D display achieved through diffuse light (1). SEM images of the display unit and a 3 pixel \times 3 pixel unit, where each pixel consists of 5×5 nanopillars (2)^[241].

The decryption process, based on a physical key and colored vortex beams, is illustrated in Fig. 16(a) (3). Photon key A consists of a 3×3 array of CVB units. White light passing through A is then encoded with different information-carrying vortex-colored beams, enabling decryption of color, OAM, and spatial information.

On the other hand, planar optical devices based on nanostructures are crucial for implementing optical steganography.

Hu *et al.* designed a volcano-shaped plasma structure using femtosecond laser printing and demonstrated its application in angle-dependent hidden color images^[251]. The schematic diagram of angle-dependent steganography is illustrated in Fig. 16(b) (1). On an MIM structure composed of a 40 nm thick Ti layer, a 126 nm Si_3N_4 dielectric layer, and an 80 nm thick Ag layer, fs laser pulses were used to irradiate the Ti layer, allowing precise control of laser power to print volcano-shaped

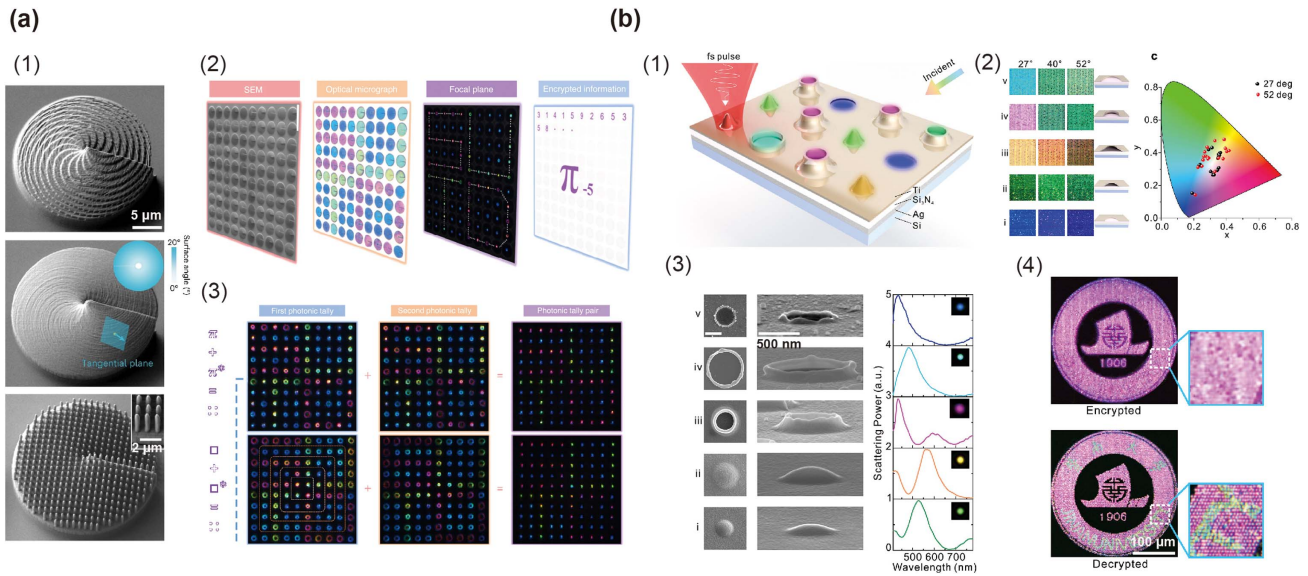


Fig. 16 Applications of structural color in optical encryption. (a) Advanced optical encryption design combining orbital angular momentum (OAM). SEM image of a single CVB unit (1). Individual control of color and OAM information on a single surface (2). Optical decryption process based on physical keys (3)^[250]. (b) Laser-induced volcano-like nanostructures on MIM surfaces (1), volcano structures showing significant angular anisotropy (2), precise control of nanostructure size by adjusting laser power (3), and utilizing volcano-like nanostructures for advanced optical steganography (4)^[251].

nanostructures of different morphologies and heights on the MIM surface, as shown in Fig. 16(b) (3). Structures of different morphologies and heights exhibit angle-dependent structural colors, as depicted in Fig. 16(b) (2). This characteristic is exploited to achieve angle-dependent image steganography, as shown in Fig. 16(b) (4), where the sample displays different colors and information at incident angles of 27° and 52°.

Owing to the strong control of light at subwavelength scales, metasurfaces have been extensively researched for their multi-dimensional optical modulation capabilities. Through the unique design of metasurface units, researchers have achieved multiple functionalities on a single metasurface. Among these functionalities, the realization of two-dimensional or three-dimensional holographic image reconstruction through phase modulation has garnered significant attention in display technology^[252–254]. To extend the applications to areas such as advanced optical encryption and higher-density optical information storage, it becomes crucial to simultaneously modulate spatial phase and spectral response within a single-layer metasurface^[255–261].

Kim *et al.* proposed an advanced encryption metasurface that combines structural colors and vector holography^[262]. In this design, the metasurface unit serves as both a Mie resonator to generate structural colors and a local half-wave plate for phase control. The control of Mie resonance is determined by the geometric parameters of the nanopillars, and the phase is achieved through geometric phase, only related to the rotation angle of the nanopillars. Therefore, it is possible to simultaneously design a single metasurface device that incorporates color, amplitude, and phase information, as shown in Fig. 17(a) (1). Nine different phase control units were designed based on the incident left- or right-circularly polarized (LCP or RCP) light, and these units were constructed into a metapixel to generate nine

polarization states, as shown in Fig. 17(a) (2). To simplify the control of holographic polarization information, LC units were integrated into the metasurface. By applying voltage to the LC units, switching between different phase gradient holographic information displays could be achieved, as shown in Fig. 17(a) (3). This design can be used as an optical encryption anti-counterfeiting label, using structural color as the primary encryption and holographic images as the secondary encryption, thereby realizing a more advanced optical anti-counterfeiting process.

Unlike conventional methods that simultaneously control amplitude and phase through a single surface, Hu *et al.* designed a three-dimensional integrated metasurface^[263]. They integrated dielectric nanohole structures for phase modulation on a Fabry-Perot (FP)-cavity-based filter, allowing for separate modulation of amplitude and phase. This design provides more degrees of freedom, enabling features like low crosstalk, high efficiency, and simple configuration. The schematic of the three-dimensional integrated metasurface is shown in Fig. 17(b) (1). The structural color part is composed of an Ag/HSQ/Ag FP cavity on a quartz substrate. The 150 nm thick HSQ serves as the spacer layer between the filter and the phase plate, with phase modulation achieved through PMMA hole structures. Different-colored FP cavity structures can serve as different color channels. By combining grayscale monochromatic images from RGB channels, a full-color holographic image can be obtained, as illustrated in Fig. 17(b) (2).

5.3 Coating or Ink

In everyday life, the extensive use of dyes is commonplace. Traditional chemical pigment synthesis often struggles to produce colors that are vibrant and bright enough, and it is plagued

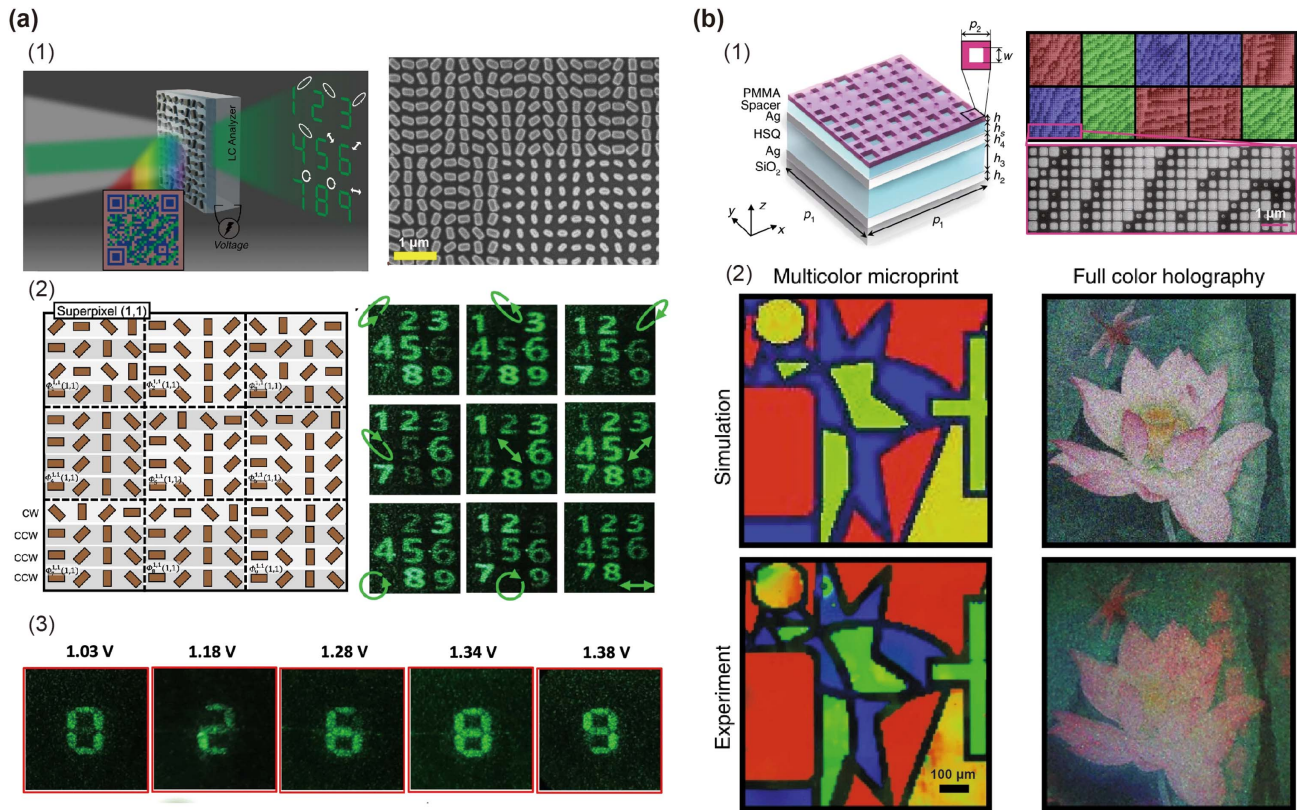


Fig. 17 Applications of structural color in the field of multiple information. (a) Metasurface enabling both structural color and holographic display of multiple information (1), multiple nanostructures forming a unit cell, modulation of holographic image information through integrated LC (2), and combining structural color with voltage-driven holographic images for multiple information transfer and advanced optical encryption (3)^[262]. (b) 3D integrated metasurface for high-performance multi-functional displays. Metasurface structure shiyitu1 and SEM image (1). Simulation design and actual structural color with holographic images (2)^[263].

by issues of fading. Moreover, the synthesis process is associated with environmental concerns related to pollution and recycling. The use of structural colors as a replacement for traditional pigments in daily applications, such as color coatings and ink printing, has long been a major goal in the field of structural colors^[264–268].

Demirörs *et al.* designed an isotropic structural color generated by photonic colloidal glass^[269]. The colloidal ink used for printing is a copolymer formed by SiO₂ nanoparticles, carbon black, and gel. Carbon black serves as an absorbing medium to reduce multiple scattering, while the gel controls the rheological behavior of the ink. These inks can achieve both the 3D shaping of colloidal glass and self-assembly. The printing process is illustrated in Fig. 18(a) (1). After printing the structure, heating is applied to remove the liquid phase and gel from the ink, resulting in the formation of colloidal glass and the generation of isotropic structural colors. The color can be adjusted by changing the size of the SiO₂ particles in the ink, as shown in Fig. 18(a) (2). This ink design can be adapted for different printing devices by adjusting the volume fraction of the nanoparticles. Furthermore, the structural color ink employs non-toxic and sustainable components, addressing pollution issues associated with traditional chemical dyes.

To enhance the practicality of structural colors in the field of coatings, it is necessary to design nanostructures that are

insensitive to polarization and achieve a large viewing angle. Figure 18(b) illustrates a structural design based on gap plasmons to achieve polarization and angle insensitivity^[87]. As depicted in Fig. 18(b) (1), an absorption layer consisting of self-assembled Al nanoparticles, a dielectric layer, and an Al back mirror collectively generates colors in a subwavelength resonant cavity. At sufficiently low electron beam evaporation rates, Al atoms self-assemble on the oxide substrate, forming small clusters of nanoparticles. The size of the nano islands can be controlled by adjusting the deposition time. Therefore, this self-assembly property can be utilized to achieve large-scale structural color fabrication using a deposition-only process. Fig. 18(b) (2) demonstrates the color display capability of the sample with polarization and angle insensitivity. Since this structure achieves structural colors through a subtractive color scheme, a single-layer structure cannot produce green. Therefore, green is achieved by using multiple layers of Al plasmons, resulting in the final color distribution as shown in Fig. 18(b) (3). Additionally, the authors created independent bidirectional color flakes on both sides of the Al back mirror and crushed them to produce powder, which can be stored in air or organic solvents, forming a structural color coating, as shown in Fig. 18(b) (4). Due to the thickness of the coating being maintained at the level of 100 nm, it can reach an astonishing 0.4 g/m². While being hundreds of times lighter than traditional

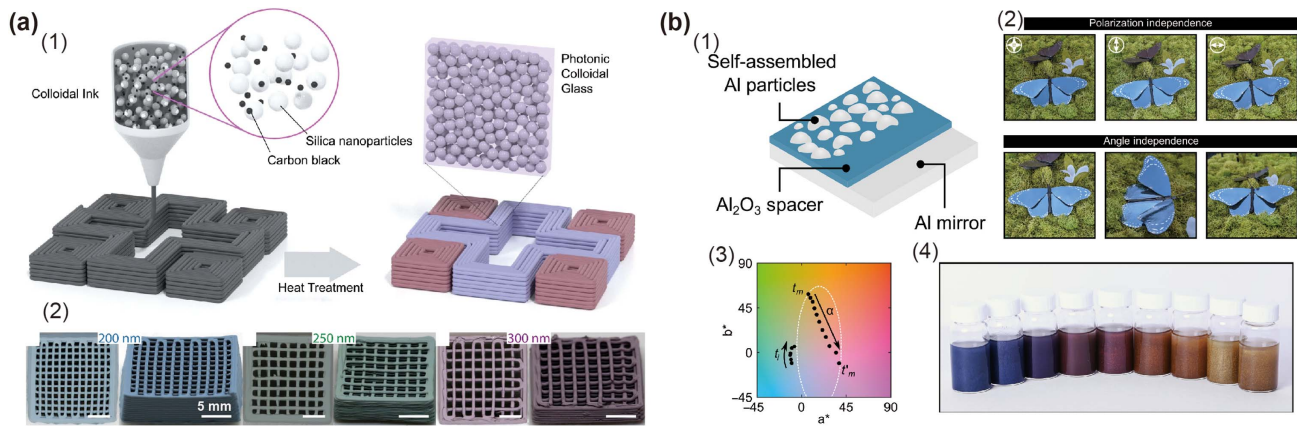


Fig. 18 Applications of structural color in coatings and ink fields. (a) Preparation of ink with mixed silica nanoparticles for printing, removing excess liquid phase by heat treatment (1), and easy adjustment of ink color by changing nanoparticle diameter (2)^[269]. (b) Self-assembled Al nanoparticles on alumina surfaces for creating plasmas used in the preparation of super-light coatings (1), due to the isotropic nature of self-assembled particles, exhibiting polarization- and angle-insensitive properties (2), controlling color by adjusting the deposition time of Al atoms (3), and preparation of super-light coatings with only 0.4 g/m² in organic solvents (4)^[87].

pigments, it can provide a more environmentally friendly and stable color display.

5.4 Sensor

The dynamic and reversible control achievable by externally modulating the nanostructures responsible for structural colors makes them sensitive to external stimuli. This characteristic has led to the application of structural colors in sensing, with extensive research focusing on applications such as motion sensing^[270], tensile and shear stress sensing^[271,272], passive humidity sensing^[273–275], gas sensing^[196,276], refractive index sensing^[277], PH sensing^[278], spectrometers^[279,280], and temperature sensing^[85,181,212]. In contrast to physical and chemical sensing, biological sensing often involves complex processes, lengthy detection times, and challenges in achieving real-time monitoring. The real-time color changes exhibited by structural colors in response to biological samples significantly reduce the complexity and time of biological detection, enabling easy implementation of real-time monitoring. Structure-color-based biosensors have been widely researched and commercialized due to these advantages^[281–285].

Metal SPP modes can generate vivid structural colors, and the resonances of localized surface plasmons exhibit sensitivity to changes in the refractive index of the surrounding environment. Therefore, SPP-based structural colors are widely researched in areas such as biological imaging and biochemical analysis^[286–288]. In the field of biology, traditional cell staining methods allow observation of different parts of cells by staining, but this process inevitably damages the cells. Therefore, achieving non-destructive observation of the living state and internal conditions of active cells has been a longstanding challenge. Brian's research team designed a patterned array of Ag nano-holes, referred to as "nanoslides," and introduced them into a cell microscopy system, enabling non-destructive color observation of live cell slices under an optical system^[289]. The biological microscopy slice model based on nanoslides is depicted in Fig. 19(a) (1). Nanoslides consist of an Ag nanohole array

covered with a protective layer of approximately 10 nm thick SiO₂. As the SPP modes are highly sensitive to changes in the dielectric constant, different regions of the biological slice cause varying degrees of redshift in the SPP mode wavelength, resulting in distinct color changes. To test the optical contrast of nanoslides, Pt/C with thicknesses of 3, 8, 13, and 19 nm was deposited on the SPP sample surface for testing. As illustrated in Fig. 19(a) (2), nanoslides exhibited a resolution sensitivity exceeding 3 nm. The ability to determine the dielectric constant of materials based on color changes was also validated by the authors. When applied to the observation of human epithelial cell slices, cancerous cell tissues exhibited significantly different color responses compared to normal cell tissues. This design holds promise for further applications in rapid pathological detection of certain diseases.

On another note, structural colors have garnered widespread attention in the field of biosensing due to their distinct color changes, low sample requirements, rapidity, and being visualizable, among other advantages. Nguyen *et al.* developed a controllable gap plasmon color film (GPCF) by combining metal nanostructures with M13 bacteriophage for the detection of volatile organic compounds (VOCs), aiming at diagnosing lung cancer through color changes in the sensor^[290]. As illustrated in Fig. 19(b) (1), the M13 bacteriophage layer acts as a modulator placed between the Ag reflector and Ag nano-cube structure. By using M13 bacteriophages modified with four different proteins and different biological layers with thicknesses of 20, 30, and 40 nm for each, a colorimetric array based on plasmonic color films was designed. The GPCF was tested for its response to various organic compounds and their concentrations, revealing a unique response to different organic molecules and concentrations. Thus, through result analysis, it can achieve identification and concentration determination of individual gases, enabling quantitative analysis as shown in Fig. 19(b) (2). Furthermore, by using the structural colors resulting from the interaction of breath gases from lung cancer patients with the colorimetric array as training samples for a convolutional neural network (CNN), the CNN model achieved discrimination

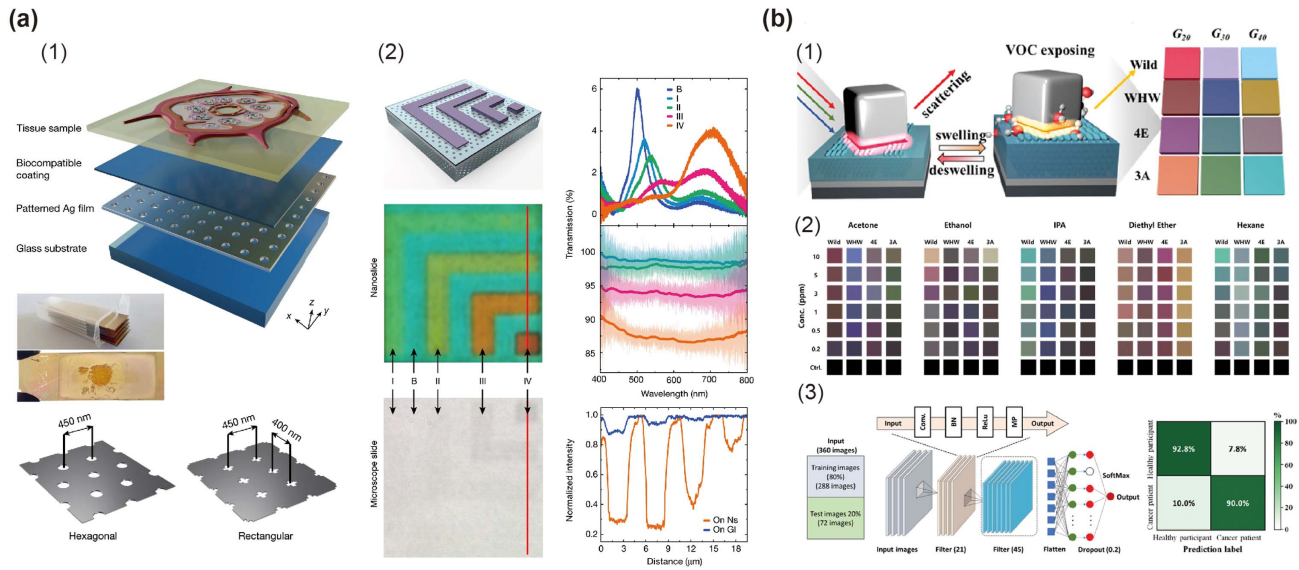


Fig. 19 Applications of structural color in the field of biosensors. (a) Cellular color observation based on structural color of metal metasurfaces. Biological slice model based on nanoslides, and two different designs of metasurface models (1). Testing with nanoslides for different thicknesses of Pt/C, showing significant color differences for 3, 8, and 19 nm, achieving a resolution of over 3 nm²[289]. (b) Plasmonic structure based on M13 bacteriophage as a biological medium for lung cancer detection (1), validation of color array for quantitative and qualitative analysis of different organic compounds (2), and combining DNN training to achieve 90% accuracy in disease diagnosis (3)^[290].

between lung cancer patients and healthy participants with accuracies of 90% and 92.8%, as illustrated in Fig. 19(b) (3). GPCF enables rapid preliminary detection of diseases, providing a relatively fast and accurate health monitoring sensor for real-time monitoring. However, biomedical monitoring often requires higher precision, and existing SPP-based biosensors still struggle to meet the high-precision quantitative analysis required for practical medical applications. In pursuit of higher detection accuracy, more sensitive optical modes, such as continuum-bound states, can be employed. Altug and colleagues established an outstanding and versatile sensing platform using BIC modes in the near-infrared wavelength range^[291]. However, further research and design are still needed for the application of visualizing BIC-based biosensing in the visible light spectrum.

6 Challenges and Opportunities

Although structural colors have achieved numerous research breakthroughs and show great potential in many fields, their main challenge for commercialization and industrialization lies in the difficulty of achieving low-cost, large-area fabrication. While large-area structural colors can be achieved through the self-assembly of nanoparticles, this method often results in isotropic structures, producing structural colors with large observation angles and polarization insensitivity^[292–296]. Due to its simplicity in preparation and the generation of isotropic structures, nanoparticle self-assembly is well-suited for applications in coatings, inks, and similar fields^[87,297]. However, self-assembly often comes with limitations in color capabilities and weak control over the light field, making it insufficient for applications requiring high color saturation and functional color displays. On the other hand, structural colors based on traditional micro-nano processes often involve EBL and etching processes,

making large-area fabrication challenging and expensive. To address these challenges, researchers are exploring large-area and low-cost micro-nano fabrication processes. Pattern transfer techniques based on nanoimprint lithography, as well as micro-nano-scale additive manufacturing techniques, hold promise for the practical application of structural colors^[94,298–300].

Nanoimprint lithography includes various processes such as contact imprinting and roll-to-roll nanoimprinting. This technique replaces traditional exposure and development steps with high-precision nano-stamps made by EBL or photolithography. It enables the large-area, high-precision, low-cost, and stable fabrication of nanostructures^[301–305]. In contact imprinting, as shown in Fig. 20(a) (1), the template is directly pressed onto the photoresist and cured, transferring the pattern onto the photoresist^[100]. To achieve faster and larger-scale sample preparation, roll-to-roll nanoimprint technology has been proposed based on contact imprinting^[306]. As illustrated in Fig. 20(a) (2)^[307], the roll-to-roll process can easily achieve continuous imprinting of 4-inch substrates with 300 nm linewidth nano-gratings on both flexible and rigid substrates, making it suitable for large-scale and rapid industrial production.

Similar to macro-scale 3D printing technology, additive manufacturing techniques at the micrometer and sub-micrometer scale have matured over time^[308,309]. 3D printing technology enables the fabrication of complex 3D structures at scales ranging from micrometers to sub-micrometers, attracting significant attention in the field of structural colors^[310–312]. Depending on the material used for structural color, there are several approaches. The simplest method involves using a conventional 3D printing nozzle to directly print polymer materials, as shown in Fig. 20(b) (1)^[313,314]. Another 3D printing approach involves using resin-based composite nanoparticle materials for printing,

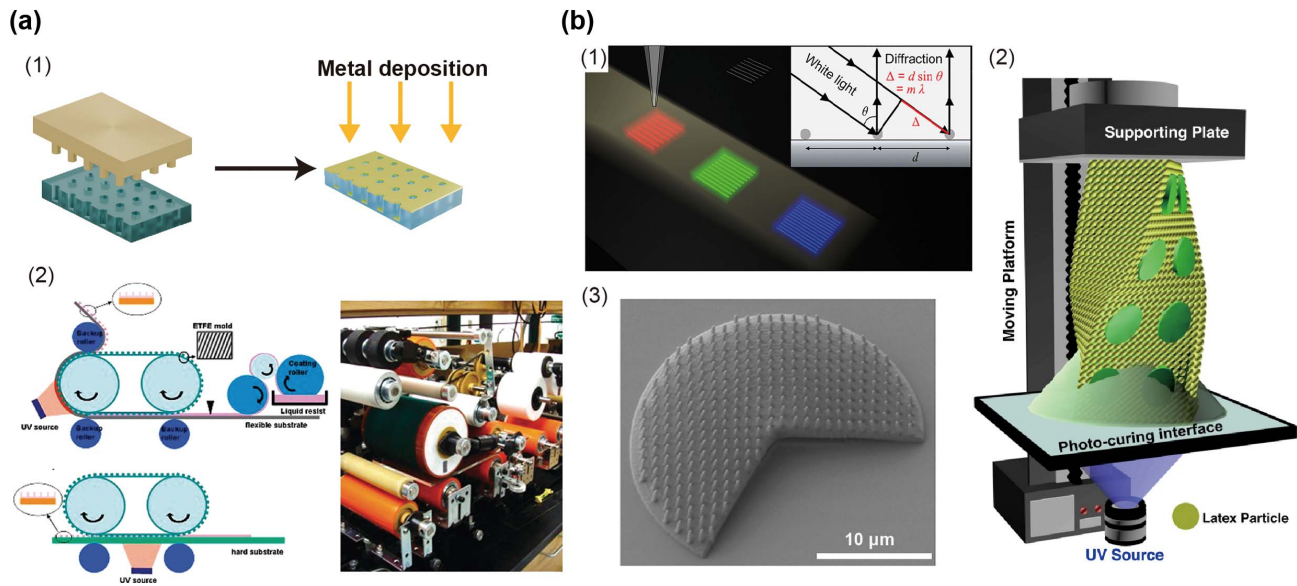


Fig. 20 Achieving large-scale structural color production based on nanoimprinting and 3D printing. (a) Structural color technology based on nanoimprinting. Schematic representation of large-area pattern transfer using nanoimprint stamps (1)^[100]. Large-area and rapid preparation using roll-to-roll nanoimprint (2)^[307]. (b) structural color technology based on 3D printing. Grating structure achieved by direct inkjet printing (1)^[313]. Structural color 3D printing using resin with composite nanoparticles (2)^[314]. Preparation of metasurface structural color based on two-photon polymerization (3)^[316].

followed by sintering to achieve vitrification^[315]. By controlling the size of the nanoparticles, color adjustment can be achieved, as depicted in Fig. 20(b) (2)^[316]. Another method is based on direct polymerization of low-refractive-index photoresist materials to form structural colors. This approach utilizes 3D printing equipment based on two-photon polymerization, enabling high processing precision, relatively fast production, and large-area structural color manufacturing, as illustrated in Fig. 20(b) (3)^[317].

While structural colors are encountering tremendous challenges that prevent them from being competitive in existing applications, they can find opportunities in next-generation technologies ranging from telecommunications to artificial intelligence. We want to emphasize that the research on structural colors is essentially developing powerful processors for spectral information with extremely high spatial resolution and spectral accuracy. Although developed originally for visible light, the spectral processing capabilities of structural coloration are transferrable to all parts of the spectrum, including the terahertz waves that are expected to be the range for 6G wireless communications^[318,319]. The ability to modulate the spectral information with high spatial resolution can become a game-changing technique for enabling high-throughput information processing for both free-space and fiber-optics systems. Structural coloration methods can also play a key role in optical computing systems (diffractive neural networks in particular)^[320] to promote fast, massively parallel computation for deep learning and machine-vision tasks^[321]. In particular, the unique ability of structural coloration systems to realize precise spectral modulation is essential for ensuring the computing accuracy of these analog systems^[322]. The synergistic development of all-optical machine learning systems and structural coloration can realize numerous AI-driven applications ranging from parallel linear transformations to quantitative phase imaging^[323,324].

We also want to point out that, although structural colors are outcompeted by existing technology for the current state-of-display industry, they are expected to become advantageous eventually because of the on-going trends for promoting the energy-efficient, miniaturized display systems. For example, structural colors may play a key role in the future commercialization of microdisplays due to the human pursuit of near-eye displays with low energy consumption, high resolution, and higher integration of microdisplays, which cannot be achieved by existing display technology. This is especially relevant as the technology advances. On the other hands, structural color has potential applications beyond traditional color displays, including in sensor devices. The tunability of micro-nanostructures allows for color changes in response to weak external stimuli, making it a useful signal change. For instance, combining structural color with biomedical detection and imaging could be beneficial. Furthermore, structural color does not require electricity to function and can rely solely on ambient light to create a sensing display. This makes structure-color-based sensor devices highly applicable due to their non-energy-dependent properties.

7 Summary and Outlook

Overall, the research on structural color has progressed tremendously in the past few years with key advances in both the discovery of fundamental mechanisms and the development of nanofabrication techniques, which have been applied to an increasingly diverse range of materials. The preliminary technology outcomes of this research are promising, particularly with regards to improvements in saturation, brightness, and resolution in displays, and reduction in system complexity for many sophisticated optical systems in information and sensing.

However, multiple challenges, both design and experimental, still have to be overcome for continued development.

(1) From the design methods perspective, the design of resonant nanostructures is often high-dimensional. It could involve many freedoms in nanostructures, including the geometry and arrangement of meta-atoms, selection of constituent materials, number of layers, state of illumination light (angle of incidence, state of polarization), methods of observation, etc. The incorporation of artificial intelligence and machine learning techniques can greatly facilitate the optimized device design corresponding to a specific color generation target. However, current outputs of topology optimization are often trapped in a local minimum due to the sheer number of parameters involved. The artificial intelligence relies excessively on computational procedures, and the lack of a physical interpretation of the resonance behavior of nanostructures will lead to an inability to obtain optima for a wide design range. In addition to processing the response corresponding to the wavelength for the target color, color generation also needs to process responses over a wide range of wavelengths beyond the target wavelength. This would go a long way towards enabling more sophisticated meta-elements and it necessitates plenty of computational resources and time. The development of machine learning can compute directly by merely specifying the design targets without time-consuming optimization procedures and an ultra-wide working frequency with high average accuracy. However, machine learning combined with metaheuristic methods and dimension reduction techniques such as diffusion maps promises to provide a solution for future inverse engineering.

(2) To increase the commercial viability of structural color based on nanostructures, cost-effective processes need to be employed. In order to ensure the resolution of the nano-scale structure, electron-beam lithography (EBL) and focused ion beams (FIBs) are typically used. In order to further adapt to the manufacturing of large-area and three-dimensional samples, another faster and more convenient avenue, direct laser printing, has also been involved. However, the throughput is extremely limited for the mentioned methods. Mass production techniques such as nanoimprinting, roll-to-roll nanoimprinting, injection molding, embossing, and large-area chemical/physical vapor deposition techniques need to be introduced. The special research for materials, photoresist, and process still needs to be conducted.

(3) The integration of structural color nanostructures with electronic-chip manufacturing, including, but not limited to, CMOS chips, including light sources, modulators, and detectors, is key to pursuing the applications for structural colors. Nanostructure-based structural color has the natural advantage of planar photonics. By integrating the structural color nanostructures directly on a CMOS chip, compact and highly integrated devices can be obtained, which not only outperform current display methods, but show the potential for application of optical devices in a wide range of fields from optical information to medical sensing. As the compact, targeted wavelength region enables the performance of high-quality tasks through structural colors, intrinsic compatibility with chips will pave the way for a completely new generation of efficient functional optical elements for a new generation of edge devices with a wide range of applications. Because the working wavelength of structural color is mainly focused on visible light, the resolution of the nanostructure is far larger than the current CMOS

chip, which is already reduced to sub-10 nm. Therefore, with appropriate design and suitable materials to eliminate pollution, the use of a CMOS-compatible fabrication process to manufacture structural color nanostructures will be a significant trend in the future.

Acknowledgments

This work was supported by the National Key Research and Development Project of China (Nos. 2022YFA1404700, 2023YFB2806700, and 2021YFA1400802), the National Natural Science Foundation of China (Nos. 6233000076, 12334016, 12025402, 62125501, 11934012, 12261131500, 92250302, and 62375232), and the Shenzhen Fundamental Research Project (Nos. JCYJ20210324120402006, JCYJ20220818102218040, GXWD20220817145518001, JCYJ20200109112805990, and JCYJ20200109113003946).

References

1. S. E. Palmer *et al.*, "Visual aesthetics and human preference," *Annu. Rev. Psychol.* **64**, 77 (2013).
2. M. Taniguchi and J. S. Lindsey, "Synthetic chlorins, possible surrogates for chlorophylls, prepared by derivatization of porphyrins," *Chem. Rev.* **117**, 344 (2017).
3. D. Zhao and J. Tao, "Recent advances on the development and regulation of flower color in ornamental plants," *Front Plant Sci.* **6**, 261 (2015).
4. P. Vukusic and J. R. Sambles, "Photonic structures in biology," *Nature* **424**, 852 (2003).
5. N. Okada *et al.*, "Rendering Morpho butterflies based on high accuracy nano-optical simulation," *J. Opt.* **42**, 25 (2013).
6. P. Vukusic *et al.*, "Structural colour - Colour mixing in wing scales of a butterfly," *Nature* **404**, 457 (2000).
7. C. Finet *et al.*, "Multi-scale dissection of wing transparency in the clearwing butterfly *Phanus vitreus*," *J. R. Soc. Interface* **20**, 20230135 (2023).
8. J. Zi *et al.*, "Coloration strategies in peacock feathers," *Proc. Natl. Acad. Sci.* **100**, 12576 (2003).
9. F. Liu *et al.*, "Inconspicuous structural coloration in the elytra of beetles *Chlorophila obscuripennis* (Coleoptera)," *Phys. Rev. E* **77**, 012901 (2008).
10. J. Teyssier *et al.*, "Photonic crystals cause active colour change in chameleons," *Nat. Commun.* **6**, 6368 (2015).
11. S. O. Aston *et al.*, "Jet printing with reactive dyes," *J. Soc. Dyers Colour.* **109**, 147 (1993).
12. G. K. Starkweather, "Electronic color printing technology," in *COMPCON '96. Technologies for the Information Superhighway Digest of Papers* 435 (1996).
13. J. Chen *et al.*, "Eco-friendly color printing using transparent wood paper," *Adv. Opt. Mater.* **11**, 2203093 (2023).
14. V. Caligiuri *et al.*, "Biodegradable and insoluble cellulose photonic crystals and metasurfaces," *ACS Nano* **14**, 9502 (2020).
15. J. Zhou *et al.*, "Self-healable organogel nanocomposite with angle-independent structural colors," *Angew. Chem. Int. Ed.* **56**, 10462 (2017).
16. A. Espinha *et al.*, "Hydroxypropyl cellulose photonic architectures by soft nanoimprinting lithography," *Nat. Photonics* **12**, 343 (2018).
17. C.-H. Lee *et al.*, "Near-ultraviolet structural colors generated by aluminum nanodisk array for bright image printing," *Adv. Opt. Mater.* **6**, 1800231 (2018).
18. Y. He *et al.*, "Precise assembly of highly crystalline colloidal photonic crystals inside the polyester yarns: a spray coating synthesis for breathable and durable fabrics with saturated structural colors," *Adv. Funct. Mater.* **32**, 2200330 (2022).

19. D.-Y. Li *et al.*, “Tunable structural coloration in eccentric water-in-oil-in-water droplets,” *Nano Lett.* **23**, 9657 (2023).
20. Y. Yang *et al.*, “Nanostructure-free crescent-shaped microparticles as full-color reflective pigments,” *Nat. Commun.* **14**, 793 (2023).
21. Y. Wang *et al.*, “Bio-inspired shape-memory structural color hydrogel film,” *Sci. Bull.* **67**, 512 (2022).
22. J. Perkins *et al.*, “Color tunable, lithography-free refractory metal–oxide metacoatings with a graded refractive index profile,” *Nano Lett.* **23**, 2601 (2023).
23. S. Chen *et al.*, “Tunable structural color images by UV-patterned conducting polymer nanofilms on metal surfaces,” *Adv. Mater.* **33**, 2102451 (2021).
24. N. Priscilla *et al.*, “Optical janus effect in large area multilayer plasmonic films,” *Adv. Photonics Res.* **3**, 2100333 (2022).
25. J. Li *et al.*, “Tunable structural colors in all-dielectric photonic crystals using energetic ion beams,” *Opt. Express* **30**, 23463 (2022).
26. H. S. Kang *et al.*, “Printable and rewritable full block copolymer structural color,” *Adv. Mater.* **29**, 1700084 (2017).
27. Y. Wang *et al.*, “Synthesis of ultrathin TiO₂/Ti films with tunable structural color,” *Appl. Opt.* **55**, 10002 (2016).
28. A. S. Rana *et al.*, “Engineering the absorption spectra of thin film multilayer absorbers for enhanced color purity in CMY color filters,” *Opt. Mater. Express* **10**, 268 (2020).
29. B. Wu *et al.*, “Large-scale reflective optical Janus color materials,” *Nanotechnology* **31**, 225301 (2020).
30. S. Miao *et al.*, “Freeze-derived heterogeneous structural color films,” *Nat. Commun.* **13**, 4044 (2022).
31. J. Zhang *et al.*, “Sessile microdroplet-based writing board for patterning of structural colored hydrogels,” *Adv. Mater. Interfaces* **8**, 2001201 (2021).
32. W. Fan *et al.*, “Iridescence-controlled and flexibly tunable retro-reflective structural color film for smart displays,” *Sci. Adv.* **5**, eaaw8755 (2019).
33. Y.-W. Huang *et al.*, “Gate-tunable conducting oxide metasurfaces,” *Nano Lett.* **16**, 5319 (2016).
34. Q. Fan *et al.*, “Independent amplitude control of arbitrary orthogonal states of polarization via dielectric metasurfaces,” *Phys. Rev. Lett.* **125**, 267402 (2020).
35. A. C. Overvig *et al.*, “Dielectric metasurfaces for complete and independent control of the optical amplitude and phase,” *Light Sci. Appl.* **8**, 92 (2019).
36. X. Xie *et al.*, “Generalized pancharatnam-berry phase in rotationally symmetric meta-atoms,” *Phys. Rev. Lett.* **126**, 183902 (2021).
37. M. R. Akram *et al.*, “Ultrathin single layer metasurfaces with ultra-wideband operation for both transmission and reflection,” *Adv. Mater.* **32**, 1907308 (2020).
38. A. Arbabi *et al.*, “Dielectric metasurfaces for complete control of phase and polarization with subwavelength spatial resolution and high transmission,” *Nat. Nanotechnol.* **10**, 937 (2015).
39. E. Maguid *et al.*, “Photonic spin-controlled multifunctional shared-aperture antenna array,” *Science* **352**, 1202 (2016).
40. R. C. Devlin *et al.*, “Arbitrary spin-to-orbital angular momentum conversion of light,” *Science* **358**, 896 (2017).
41. B. Wang *et al.*, “Generating optical vortex beams by momentum-space polarization vortices centred at bound states in the continuum,” *Nat. Photonics* **14**, 623 (2020).
42. K. Kumar *et al.*, “Printing colour at the optical diffraction limit,” *Nat. Nanotechnol.* **7**, 557 (2012).
43. D. Franklin *et al.*, “Actively addressed single pixel full-colour plasmonic display,” *Nat. Commun.* **8**, 15209 (2017).
44. D. Franklin *et al.*, “Self-assembled plasmonics for angle-independent structural color displays with actively addressed black states,” *Proc. Natl. Acad. Sci.* **117**, 13350 (2020).
45. K. V. Sreekanth *et al.*, “Electrically tunable all-PCM visible plasmonics,” *Nano Lett.* **21**, 4044 (2021).
46. S. G.-C. Carrillo *et al.*, “A nonvolatile phase-change metamaterial color display,” *Adv. Opt. Mater.* **7**, 1801782 (2019).
47. S. Song *et al.*, “Actively tunable structural color rendering with tensile substrate,” *Adv. Opt. Mater.* **5**, 1600829 (2017).
48. Q. Ruan *et al.*, “Reconfiguring colors of single relief structures by directional stretching,” *Adv. Mater.* **34**, 2108128 (2022).
49. M. Song *et al.*, “Enabling optical steganography, data storage, and encryption with plasmonic colors,” *Laser Photonics Rev.* **15**, 2000343 (2021).
50. L. Li *et al.*, “High-saturation full-color printing with all-dielectric chiral metasurfaces,” *ACS Appl. Mater. Interfaces* **1**, 1301 (2023).
51. J. Gu *et al.*, “Structural colors based on diamond metasurface for information encryption,” *Adv. Opt. Mater.* **11**, 2202826 (2023).
52. C. Jung *et al.*, “Near-zero reflection of all-dielectric structural coloration enabling polarization-sensitive optical encryption with enhanced switchability,” *Nanophotonics* **10**, 919 (2021).
53. S. Choi *et al.*, “Chirality-selective all-dielectric metasurface structural color display,” *Opt. Express* **29**, 41258 (2021).
54. S. Jiang *et al.*, “Multilevel anti-counterfeiting based on covert structural features embedded in femtosecond-laser-treated gold nanocluster/graphene hybrid layer,” *ACS Appl. Mater. Interfaces* **14**, 39240 (2022).
55. D. Franklin *et al.*, “Covert infrared image encoding through imprinted plasmonic cavities,” *Light Sci. Appl.* **7**, 93 (2018).
56. V. Lapidis *et al.*, “Direct laser printing of high-resolution physically unclonable function anti-counterfeit labels,” *Appl. Phys. Lett.* **120**, 261104 (2022).
57. Y. Zhang *et al.*, “Full-visible multifunctional aluminium metasurfaces by in situ anisotropic thermoplasmonic laser printing,” *Nanoscale Horiz.* **4**, 601 (2019).
58. J. Y. E. Chan *et al.*, “Full geometric control of hidden color information in diffraction gratings under angled white light illumination,” *Nano Lett.* **22**, 8189 (2022).
59. L. Bai *et al.*, “Large-scale noniridescent structural color printing enabled by infiltration-driven nonequilibrium colloidal assembly,” *Adv. Mater.* **30**, 1705667 (2018).
60. X. Zhu *et al.*, “Resonant laser printing of structural colors on high-index dielectric metasurfaces,” *Sci. Adv.* **3**, e1602487 (2017).
61. L. Qin *et al.*, “Geminate labels programmed by two-tone microdroplets combining structural and fluorescent color,” *Nat. Commun.* **12**, 699 (2021).
62. Y. Zhang *et al.*, “Using cuttlefish ink as an additive to produce non-iridescent structural colors of high color visibility,” *Adv. Mater.* **27**, 4719 (2015).
63. J. B. Kim *et al.*, “Direct writing of customized structural-color graphics with colloidal photonic inks,” *Sci. Adv.* **7**, eabj8780 (2021).
64. S. S. Lee *et al.*, “Structural color palettes of core-shell photonic ink capsules containing cholesteric liquid crystals,” *Adv. Mater.* **29**, 1606894 (2017).
65. T. Wang *et al.*, “Naked eye plasmonic indicator with multi-responsive polymer brush as signal transducer and amplifier,” *Nanoscale* **9**, 1925 (2017).
66. J. Jang *et al.*, “Self-powered humidity sensor using chitosan-based plasmonic metal–hydrogel–metal filters,” *Adv. Opt. Mater.* **8**, 1901932 (2020).
67. A. Choe *et al.*, “Stretchable and wearable colorimetric patches based on thermoresponsive plasmonic microgels embedded in a hydrogel film,” *NPG Asia Mater.* **10**, 912 (2018).
68. Y.-S. Lin and W. Chen, “A large-area, wide-incident-angle, and polarization-independent plasmonic color filter for glucose sensing,” *Opt. Mater.* **75**, 739 (2018).
69. A. Kristensen *et al.*, “Plasmonic colour generation,” *Nat. Rev. Mater.* **2**, 16088 (2016).
70. L. Huang *et al.*, “Helicity dependent directional surface plasmon polariton excitation using a metasurface with interfacial phase discontinuity,” *Light Sci. Appl.* **2**, e70 (2013).

71. N. Yu *et al.*, "Light propagation with phase discontinuities: generalized laws of reflection and refraction," *Science* **334**, 333 (2011).
72. M. S. Bin-Alam *et al.*, "Ultra-high-Q resonances in plasmonic metasurfaces," *Nat. Commun.* **12**, 974 (2021).
73. A. A. High *et al.*, "Visible-frequency hyperbolic metasurface," *Nature* **522**, 192 (2015).
74. Y. Huang *et al.*, "Polarization-controlled bifunctional metasurface for structural color printing and beam deflection," *Opt. Lett.* **45**, 1707 (2020).
75. J. Lin *et al.*, "Polarization-controlled tunable directional coupling of surface plasmon polaritons," *Science* **340**, 331 (2013).
76. F. Ding *et al.*, "Broadband high-efficiency half-wave plate: a supercell-based plasmonic metasurface approach," *ACS Nano* **9**, 4111 (2015).
77. S. Y. Lee *et al.*, "Metallic nanodimple arrays for wide-angle coloration via plasmonic and structural resonances," *Chem. Mater.* **33**, 4628 (2021).
78. Y. Liu *et al.*, "Millimeter-wave E-plane waveguide bandpass filters based on spoof surface plasmon polaritons," *IEEE Trans. Microw. Theory Tech.* **70**, 4399 (2022).
79. H. F. Ma *et al.*, "Broadband and high-efficiency conversion from guided waves to spoof surface plasmon polaritons," *Laser Photonics Rev.* **8**, 146 (2014).
80. H. Kim *et al.*, "Synthesis and dynamic switching of surface plasmon vortices with plasmonic vortex lens," *Nano Lett.* **10**, 529 (2010).
81. G. Zheng *et al.*, "Metasurface holograms reaching 80% efficiency," *Nat. Nanotechnol.* **10**, 308 (2015).
82. S. Tsesses *et al.*, "Tunable photon-induced spatial modulation of free electrons," *Nat. Mater.* **22**, 345 (2023).
83. A. Smolyaninov *et al.*, "Programmable plasmonic phase modulation of free-space wavefronts at gigahertz rates," *Nat. Photonics* **13**, 431 (2019).
84. I. Freestone *et al.*, "The Lycurgus Cup — a Roman nanotechnology," *Gold Bull.* **40**, 270 (2007).
85. Y. Zhao *et al.*, "Thermosensitive plasmonic color enabled by sodium metasurface," *Adv. Funct. Mater.* **33**, 2214492 (2023).
86. H.-C. Wang and O. J. F. Martin, "Polarization-controlled chromo-encryption," *Adv. Opt. Mater.* **11**, 2202165 (2023).
87. P. Cencillo-Abad *et al.*, "Ultralight plasmonic structural color paint," *Sci. Adv.* **9**, eadf7207 (2023).
88. S. Choi *et al.*, "Structural color printing via polymer-assisted photochemical deposition," *Light Sci. Appl.* **11**, 84 (2022).
89. M. Zheng *et al.*, "Enhancing plasmonic spectral tunability with anomalous material dispersion," *Nano Lett.* **21**, 91 (2021).
90. Z. Li *et al.*, "Extremely-fine color printing by 2D materials with the synergetic effects of Fabry–Pérot cavity and exciton absorption," *Laser Photonics Rev.* **16**, 2200394 (2022).
91. G. Si *et al.*, "Reflective plasmonic color filters based on lithographically patterned silver nanorod arrays," *Nanoscale* **5**, 6243 (2013).
92. S. J. Tan *et al.*, "Plasmonic color palettes for photorealistic printing with aluminum nanostructures," *Nano Lett.* **14**, 4023 (2014).
93. J. S. Clausen *et al.*, "Plasmonic metasurfaces for coloration of plastic consumer products," *Nano Lett.* **14**, 4499 (2014).
94. L. Duempelmann *et al.*, "Color rendering plasmonic aluminum substrates with angular symmetry breaking," *ACS Nano* **9**, 12383 (2015).
95. H. Wang *et al.*, "Full color generation using silver tandem nanodisks," *ACS Nano* **11**, 4419 (2017).
96. B. Zeng *et al.*, "Ultrathin nanostructured metals for highly transmissive plasmonic subtractive color filters," *Sci. Rep.* **3**, 2840 (2013).
97. H. Hu *et al.*, "Direct growth of vertically orientated nanocavity arrays for plasmonic color generation," *Adv. Funct. Mater.* **30**, 2002287 (2020).
98. D. Inoue *et al.*, "Polarization independent visible color filter comprising an aluminum film with surface-plasmon enhanced transmission through a subwavelength array of holes," *Appl. Phys. Lett.* **98**, 093113 (2011).
99. Z. Li *et al.*, "Dual color plasmonic pixels create a polarization controlled nano color palette," *ACS Nano* **10**, 492 (2016).
100. B.-R. Lu *et al.*, "High-resolution plasmonic structural colors from nanohole arrays with bottom metal disks," *Opt. Lett.* **41**, 1400 (2016).
101. C. U. Hail *et al.*, "A plasmonic painter's method of color mixing for a continuous red-green-blue palette," *ACS Nano* **14**, 1783 (2020).
102. M. Song *et al.*, "Versatile full-colour nanopainting enabled by a pixelated plasmonic metasurface," *Nat. Nanotechnol.* **18**, 71 (2023).
103. K.-T. Lee *et al.*, "Flexible high-color-purity structural color filters based on a higher-order optical resonance suppression," *Sci. Rep.* **9**, 14917 (2019).
104. H. Pan *et al.*, "Wide gamut, angle-insensitive structural colors based on deep-subwavelength bilayer media," *Nanophotonics* **9**, 3385 (2020).
105. P. Mao *et al.*, "Manipulating disordered plasmonic systems by external cavity with transition from broadband absorption to reconfigurable reflection," *Nat. Commun.* **11**, 1538 (2020).
106. J. Kim *et al.*, "Metal-semiconductor-metal metasurface for multi-band infrared stealth technology using camouflage color pattern in visible range," *Adv. Opt. Mater.* **10**, 2101930 (2022).
107. C. Li *et al.*, "Janus structural color from a 2D photonic crystal hybrid with a Fabry–Perot cavity," *Adv. Opt. Mater.* **6**, 1800651 (2018).
108. Z. Yang *et al.*, "Reflective Color Filters and Monolithic Color Printing Based on Asymmetric Fabry–Perot cavities using nickel as a broadband absorber," *Adv. Opt. Mater.* **4**, 1196 (2016).
109. Y. Wei *et al.*, "Silicon metasurface embedded Fabry–Perot cavity enables the high-quality transmission structural color," *Opt. Lett.* **47**, 5344 (2022).
110. M. ElKabbash *et al.*, "Fano resonant optical coatings platform for full gamut and high purity structural colors," *Nat. Commun.* **14**, 3960 (2023).
111. F. Cheng *et al.*, "Structural color printing based on plasmonic metasurfaces of perfect light absorption," *Sci. Rep.* **5**, 11045 (2015).
112. A. S. Roberts *et al.*, "Laser writing of bright colors on near-percolation plasmonic reflector arrays," *ACS Nano* **13**, 71 (2019).
113. M. Miyata *et al.*, "Full-color subwavelength printing with gap-plasmonic optical antennas," *Nano Lett.* **16**, 3166 (2016).
114. J. C. Blake *et al.*, "Scalable reflective plasmonic structural colors from nanoparticles and cavity resonances—the cyan-magenta-yellow approach," *Adv. Opt. Mater.* **10**, 2200471 (2022).
115. L. Duempelmann *et al.*, "Four-fold color filter based on plasmonic phase retarder," *ACS Photonics* **3**, 190 (2016).
116. Y.-K. R. Wu *et al.*, "Angle-insensitive structural colours based on metallic nanocavities and coloured pixels beyond the diffraction limit," *Sci. Rep.* **3**, 1194 (2013).
117. L. Cheng *et al.*, "Extrinsic polarization-enabled covert plasmonic colors using aluminum nanostructures," *Ann. Phys. Lpz.* **531**, 1900073 (2019).
118. M. Jiang *et al.*, "Patterned resist on flat silver achieving saturated plasmonic colors with sub-20-nm spectral linewidth," *Mater. Today* **35**, 99 (2020).
119. W. Wang *et al.*, "Realizing structural color generation with aluminum plasmonic V-groove metasurfaces," *Opt. Express* **25**, 20454 (2017).
120. J. R. Fan *et al.*, "Three-dimensional cavity nanoantennas with resonant-enhanced surface plasmons as dynamic color-tuning reflectors," *Nanoscale* **9**, 3416 (2017).
121. S. U. Lee and B.-K. Ju, "Wide-gamut plasmonic color filters using a complementary design method," *Sci. Rep.* **7**, 40649 (2017).

122. X. Zhuo *et al.*, “Colour routing with single silver nanorods,” *Light Sci. Appl.* **8**, 39 (2019).
123. J. Jang *et al.*, “Spectral modulation through the hybridization of Mie-scatterers and quasi-guided mode resonances: realizing full and gradients of structural color,” *ACS Nano* **14**, 15317 (2020).
124. X. Liu *et al.*, “All-dielectric silicon nanoring metasurface for full-color printing,” *Nano Lett.* **20**, 8739 (2020).
125. Y. Nagasaki *et al.*, “All-dielectric dual-color pixel with subwavelength resolution,” *Nano Lett.* **17**, 7500 (2017).
126. T. Lee *et al.*, “Nearly perfect transmissive subtractive coloration through the spectral amplification of mie scattering and lattice resonance,” *ACS Appl. Mater. Interfaces* **13**, 26299 (2021).
127. J. Xiang *et al.*, “Manipulating the orientations of the electric and magnetic dipoles induced in silicon nanoparticles for multicolor display,” *Laser Photonics Rev.* **12**, 1800032 (2018).
128. J. S. Lee *et al.*, “Ultrahigh resolution and color gamut with scattering-reducing transmissive pixels,” *Nat. Commun.* **10**, 4782 (2019).
129. H. Park *et al.*, “Filter-free image sensor pixels comprising silicon nanowires with selective color absorption,” *Nano Lett.* **14**, 1804 (2014).
130. H. Li *et al.*, “All-dielectric high saturation structural colors enhanced by multipolar modulated metasurfaces,” *Opt. Express* **30**, 28954 (2022).
131. J. Lu *et al.*, “A versatile metasurface enabling superwettability for self-cleaning and dynamic color response,” *Adv. Opt. Mater.* **10**, 2101781 (2022).
132. Z. Dong *et al.*, “Printing beyond sRGB color gamut by mimicking silicon nanostructures in free-space,” *Nano Lett.* **17**, 7620 (2017).
133. Y. Han *et al.*, “Structural colored fabrics with brilliant colors, low angle dependence, and high color fastness based on the mie scattering of Cu₂O spheres,” *ACS Appl. Mater. Interfaces* **13**, 57796 (2021).
134. S. Sun *et al.*, “All-dielectric full-color printing with TiO₂ metasurfaces,” *ACS Nano* **11**, 4445 (2017).
135. D. Lin *et al.*, “Dielectric gradient metasurface optical elements,” *Science* **345**, 298 (2014).
136. V. Flauraud *et al.*, “Silicon nanostructures for bright field full color prints,” *ACS Photonics* **4**, 1913 (2017).
137. V. Vashistha *et al.*, “All-dielectric metasurfaces based on cross-shaped resonators for color pixels with extended gamut,” *ACS Photonics* **4**, 1076 (2017).
138. W. Yang *et al.*, “All-dielectric metasurface for high-performance structural color,” *Nat. Commun.* **11**, 1864 (2020).
139. M. Hentschel *et al.*, “Dielectric Mie voids: confining light in air,” *Light Sci. Appl.* **12**, 3 (2023).
140. Z. Dong *et al.*, “Schrödinger’s red pixel by quasi-bound-states-in-the-continuum,” *Sci. Adv.* **8**, eabm4512 (2022).
141. B. Yang *et al.*, “Polarization-sensitive structural colors with hue-and-saturation tuning based on all-dielectric nanopixels,” *Adv. Opt. Mater.* **6**, 1701009 (2018).
142. X. Yuan *et al.*, “Structural colour of polyester fabric coated with Ag/TiO₂ multilayer films,” *Surf. Eng.* **33**, 231 (2017).
143. Y. Xue *et al.*, “Preparation of noniridescent structurally colored PS@TiO₂ and Air@C@TiO₂ core-shell nanoparticles with enhanced color stability,” *ACS Appl. Mater. Interfaces* **11**, 34355 (2019).
144. L. Wang *et al.*, “Tunable structural colors generated by hybrid Si₃N₄ and Al metasurfaces,” *Opt. Express* **30**, 7299 (2022).
145. M. Vega *et al.*, “Color engineering of silicon nitride surfaces to characterize the polydopamine refractive index,” *ChemPhysChem* **19**, 3418 (2018).
146. M. J. Uddin and R. Magnusson, “Highly efficient color filter array using resonant Si₃N₄ gratings,” *Opt. Express* **21**, 12495 (2013).
147. H. Liu *et al.*, “Transfer printing of solution-processed 3D ZnO nanostructures with ultra-high yield for flexible metasurface color filter,” *Adv. Mater. Interfaces* **9**, 2101963 (2022).
148. H. Liu *et al.*, “Dielectric metasurface from solution-phase epitaxy of ZnO nanorods for subtractive color filter application,” *Adv. Opt. Mater.* **9**, 2001670 (2021).
149. Z. Li *et al.*, “Application of nanostructured TiO₂ in UV photo-detectors: a review,” *Adv. Mater.* **34**, 2109083 (2022).
150. B. Bharti *et al.*, “Formation of oxygen vacancies and Ti³⁺ state in TiO₂ thin film and enhanced optical properties by air plasma treatment,” *Sci. Rep.* **6**, 32355 (2016).
151. J. Wang *et al.*, “A review on TiO₂-x-based materials for photocatalytic CO₂ reduction,” *Nanoscale* **14**, 11512 (2022).
152. B. Yang *et al.*, “Ultrahighly saturated structural colors enhanced by multipolar-modulated metasurfaces,” *Nano Lett.* **19**, 4221 (2019).
153. X. Huang *et al.*, “All-dielectric metasurfaces color filter arrays designed by evolutionary search,” *IEEE Photonics J.* **13**, 1 (2021).
154. S. S. Panda and R. S. Hegde, “Transmission-mode all-dielectric metasurface color filter arrays designed by evolutionary search,” *J. Nanophotonics* **14**, 1 (2020).
155. T. Phan *et al.*, “High-efficiency, large-area, topology-optimized metasurfaces,” *Light Sci. Appl.* **8**, 48 (2019).
156. S. S. Panda *et al.*, “Robust inverse design of all-dielectric metasurface transmission-mode color filters,” *Opt. Mater. Express* **10**, 3145 (2020).
157. S. So *et al.*, “Multicolor and 3D holography generated by inverse-designed single-cell metasurfaces,” *Adv. Mater.* **35**, 2208520 (2023).
158. R. Zhu *et al.*, “Phase-to-pattern inverse design paradigm for fast realization of functional metasurfaces via transfer learning,” *Nat. Commun.* **12**, 2974 (2021).
159. W. Ma *et al.*, “Pushing the limits of functionality-multiplexing capability in metasurface design based on statistical machine learning,” *Adv. Mater.* **34**, 2110022 (2022).
160. O. Khatib *et al.*, “Learning the physics of all-dielectric metamaterials with deep lorentz neural networks,” *Adv. Opt. Mater.* **10**, 2200097 (2022).
161. Y. Chen and L. Dal Negro, “Physics-informed neural networks for imaging and parameter retrieval of photonic nanostructures from near-field data,” *APL Photonics* **7**, 010802 (2022).
162. Y. Tang *et al.*, “Physics-informed recurrent neural network for time dynamics in optical resonances,” *Nat. Comput. Sci.* **2**, 169 (2022).
163. Y. Chen *et al.*, “Physics-informed neural networks for inverse problems in nano-optics and metamaterials,” *Opt. Express* **28**, 11618 (2020).
164. L. Xu *et al.*, “Enhanced light-matter interactions in dielectric nanostructures via machine-learning approach,” *Adv. Photonics* **2**, 026003 (2020).
165. J. Li *et al.*, “Single-sized metasurface for simultaneous pseudo-color nanoprinting and holographic image display,” *Front. nanotechnol.* **4**, 973348 (2022).
166. P. Pillai *et al.*, “Modified variational autoencoder for inversely predicting plasmonic nanofeatures for generating structural color,” *Sci. Rep.* **13**, 3536 (2023).
167. H. Ma *et al.*, “Predicting laser-induced colors of random plasmonic metasurfaces and optimizing image multiplexing using deep learning,” *ACS Nano* **16**, 9410 (2022).
168. J. Baxter *et al.*, “Plasmonic colours predicted by deep learning,” *Sci. Rep.* **9**, 8074 (2019).
169. N. B. Roberts and M. Keshavarz Hedayati, “A deep learning approach to the forward prediction and inverse design of plasmonic metasurface structural color,” *Appl. Phys. Lett.* **119**, 061101 (2021).
170. Z. Liu *et al.*, “Generative model for the inverse design of metasurfaces,” *Nano Lett.* **18**, 6570 (2018).

171. P. Gómez *et al.*, “Neural inverse design of nanostructures (NIDN),” *Sci. Rep.* **12**, 22160 (2022).
172. I. Sajedian *et al.*, “Optimisation of colour generation from dielectric nanostructures using reinforcement learning,” *Opt. Express* **27**, 5874 (2019).
173. A. Clini de Souza *et al.*, “Back-propagation optimization and multi-valued artificial neural networks for highly vivid structural color filter metasurfaces,” *Sci. Rep.* **13**, 21352 (2023).
174. Q. He *et al.*, “Tunable/reconfigurable metasurfaces: physics and applications,” *Research* **2019**, 1849272 (2019).
175. L. Yang *et al.*, “Rechargeable metasurfaces for dynamic color display based on a compositional and mechanical dual-altered mechanism,” *Research* **2022**, 9828757 (2022).
176. Y. Wu *et al.*, “TiO₂ metasurfaces: from visible planar photonics to photochemistry,” *Sci. Adv.* **5**, eaax0939 (2019).
177. S. Sun *et al.*, “Real-time tunable colors from microfluidic reconfigurable all-dielectric metasurfaces,” *ACS Nano* **12**, 2151 (2018).
178. L. Wang *et al.*, “Color printing and encryption with polarization-switchable structural colors on all-dielectric metasurfaces,” *Nano Lett.* **23**, 5581 (2023).
179. G. Li *et al.*, “Direction-controllable plasmonic color scanning by using laser-induced bubbles,” *Adv. Funct. Mater.* **31**, 2008579 (2021).
180. Y. Gao *et al.*, “Lead halide perovskite nanostructures for dynamic color display,” *ACS Nano* **12**, 8847 (2018).
181. Z. Li *et al.*, “Creation and reconstruction of thermochromic Au nanorods with surface concavity,” *J. Am. Chem. Soc.* **143**, 15791 (2021).
182. C. Ji *et al.*, “Quadruple anti-counterfeiting retroreflective structural color films,” *Adv. Opt. Mater.* **10**, 2102383 (2022).
183. Z. Miao *et al.*, “Widely tunable terahertz phase modulation with gate-controlled graphene metasurfaces,” *Phys. Rev. X* **5**, 041027 (2015).
184. G. Wang *et al.*, “Mechanical chameleon through dynamic real-time plasmonic tuning,” *ACS Nano* **10**, 1788 (2016).
185. Y. Li *et al.*, “Dynamic tuning of gap plasmon resonances using a solid-state electrochromic device,” *Nano Lett.* **19**, 7988 (2019).
186. M. Gugole *et al.*, “High-contrast switching of plasmonic structural colors: inorganic versus organic electrochromism,” *ACS Photonics* **7**, 1762 (2020).
187. S. Zhang *et al.*, “Electrochromic modulation of plasmonic resonance in a PEDOT-coated nanodisk metasurface,” *Opt. Mater. Express* **10**, 1053 (2020).
188. Z. Yan *et al.*, “Floating solid-state thin films with dynamic structural colour,” *Nat. Nanotechnol.* **16**, 795 (2021).
189. J. Eaves-Rathert *et al.*, “Dynamic color tuning with electrochemically actuated TiO₂ metasurfaces,” *Nano Lett.* **22**, 1626 (2022).
190. N.-N. Huang *et al.*, “Structural design of intelligent reversible two-way structural color films,” *Nano Lett.* **23**, 7389 (2023).
191. C. Wu *et al.*, “Magnetically tunable one-dimensional plasmonic photonic crystals,” *Nano Lett.* **23**, 1981 (2023).
192. L. He *et al.*, “Magnetochromatic thin-film microplates,” *Adv. Mater.* **27**, 86 (2015).
193. S. Y. Lee *et al.*, “Magneto-responsive photonic microspheres with structural color gradient,” *Adv. Mater.* **29**, 1605450 (2017).
194. M. Wang and Y. Yin, “Magnetically responsive nanostructures with tunable optical properties,” *J. Am. Chem. Soc.* **138**, 6315 (2016).
195. J. W. Kim *et al.*, “Magnetic control of the plasmonic chirality in gold helicoids,” *Nano Lett.* **22**, 8181 (2022).
196. X. Duan *et al.*, “Dynamic plasmonic colour display,” *Nat. Commun.* **8**, 14606 (2017).
197. Y. Chen *et al.*, “Dynamic color displays using stepwise cavity resonators,” *Nano Lett.* **17**, 5555 (2017).
198. H. Liu *et al.*, “Rewritable color nanoprints in antimony trisulfide films,” *Sci. Adv.* **6**, eabb7171 (2020).
199. H. Liu *et al.*, “Switchable all-dielectric metasurfaces for full-color reflective display,” *Adv. Opt. Mater.* **7**, 1801639 (2019).
200. D. Zheng *et al.*, “Metamaterial grating for colorimetric chemical sensing applications,” *Mater. Today Phys.* **33**, 101056 (2023).
201. X. Gao *et al.*, “Polarization tunable transmitted full-color display enabling switchable bright and dark states,” *Opt. Express* **31**, 3083 (2023).
202. C.-H. Park *et al.*, “Electrically tunable color filter based on a polarization-tailored nano-photonics dichroic resonator featuring an asymmetric subwavelength grating,” *Opt. Express* **21**, 28783 (2013).
203. J. Jang *et al.*, “Kerker-conditioned dynamic cryptographic nanoprints,” *Adv. Opt. Mater.* **7**, 1801070 (2019).
204. J. Cai *et al.*, “Dual-color flexible metasurfaces with polarization-tunable plasmons in gold nanorod arrays,” *Adv. Opt. Mater.* **9**, 2001401 (2021).
205. Y. Taii *et al.*, “Transparent color pixels using plastic MEMS technology for electronic papers,” *IEICE Electron. Express* **3**, 97 (2006).
206. M. L. Tseng *et al.*, “Two-dimensional active tuning of an aluminum plasmonic array for full-spectrum response,” *Nano Lett.* **17**, 6034 (2017).
207. H. Kumagai *et al.*, “Stretchable and high-adhesive plasmonic metasheet using Al subwavelength grating embedded in an elastomer nanosheet,” *Adv. Opt. Mater.* **8**, 1902074 (2020).
208. X. Cai *et al.*, “Dynamically controlling terahertz wavefronts with cascaded metasurfaces,” *Adv. Photonics* **3**, 036003 (2021).
209. O. L. Muskens *et al.*, “Antenna-assisted picosecond control of nanoscale phase transition in vanadium dioxide,” *Light Sci. Appl.* **5**, e16173 (2016).
210. D. Wegkamp and J. Stähler, “Ultrafast dynamics during the photoinduced phase transition in VO₂,” *Prog. Surf. Sci.* **90**, 464 (2015).
211. S. Wang *et al.*, “Scalable thermochromic smart windows with passive radiative cooling regulation,” *Science* **374**, 1501 (2021).
212. J. He *et al.*, “VO₂ based dynamic tunable absorber and its application in switchable control and real-time color display in the visible region,” *Opt. Express* **28**, 37590 (2020).
213. Y. Zhang *et al.*, “Electrically reconfigurable non-volatile metasurface using low-loss optical phase-change material,” *Nat. Nanotechnol.* **16**, 661 (2021).
214. S. Abdollahramezani *et al.*, “Electrically driven reprogrammable phase-change metasurface reaching 80% efficiency,” *Nat. Commun.* **13**, 1696 (2022).
215. P. Hosseini *et al.*, “An optoelectronic framework enabled by low-dimensional phase-change films,” *Nature* **511**, 206 (2014).
216. F. Ding *et al.*, “Dynamic metasurfaces using phase-change chalcogenides,” *Adv. Opt. Mater.* **7**, 1801709 (2019).
217. L. Lu *et al.*, “Reversible tuning of mie resonances in the visible spectrum,” *ACS Nano* **15**, 19722 (2021).
218. O. A. M. Abdelraouf *et al.*, “All-optical switching of structural color with a Fabry-Pérot cavity,” *Adv. Photonics Res.* **4**, 2300209 (2023).
219. V. Raj Shrestha *et al.*, “Polarization-tuned dynamic color filters incorporating a dielectric-loaded aluminum nanowire array,” *Sci. Rep.* **5**, 12450 (2015).
220. M. Kim *et al.*, “Active color control in a metasurface by polarization rotation,” *Appl. Sci.* **8**, 982 (2018).
221. D. Franklin *et al.*, “Polarization-independent actively tunable colour generation on imprinted plasmonic surfaces,” *Nat. Commun.* **6**, 7337 (2015).
222. G. M. Akselrod *et al.*, “Plasmonic surface-scattering elements and metasurfaces for optical beam steering,” *U.S. Patent No.* 10451800 (2019).
223. G. M. Akselrod *et al.*, “Tunable liquid crystal metasurfaces,” *U.S. Patent No.* 110665953 (2020).
224. K. Li *et al.*, “Electrically switchable, polarization-sensitive encryption based on aluminum nanoaperture arrays integrated with polymer-dispersed liquid crystals,” *Nano Lett.* **21**, 7183 (2021).

225. T. Badloe *et al.*, “Liquid crystal-powered Mie resonators for electrically tunable photorealistic color gradients and dark blacks,” *Light Sci. Appl.* **11**, 118 (2022).
226. M. F. Karim *et al.*, “A tunable bandstop filter via the capacitance change of micromachined switches,” *J. Micromech. Microeng.* **16**, 851 (2006).
227. Z. Han *et al.*, “MEMS cantilever-controlled plasmonic colors for sustainable optical displays,” *Sci. Adv.* **8**, eabn0889 (2022).
228. A. L. Holsteen *et al.*, “Temporal color mixing and dynamic beam shaping with silicon metasurfaces,” *Science* **365**, 257 (2019).
229. C. Zhang *et al.*, “Stretchable all-dielectric metasurfaces with polarization-insensitive and full-spectrum response,” *ACS Nano* **14**, 1418 (2020).
230. X. Hou *et al.*, “Bioinspired multichannel colorful encryption through kirigami activating grating,” *Sci. Bull.* **68**, 276 (2023).
231. C. Sun *et al.*, “Force-induced synergetic pigmentary and structural color change of liquid crystalline elastomer with nanoparticle-enhanced mechanosensitivity,” *Adv. Sci.* **9**, 2205325 (2022).
232. T. L. Williams *et al.*, “Dynamic pigmentary and structural coloration within cephalopod chromatophore organs,” *Nat. Commun.* **10**, 1004 (2019).
233. K. Li *et al.*, “Facile full-color printing with a single transparent ink,” *Sci. Adv.* **7**, eabh1992 (2021).
234. S. D. Rezaei *et al.*, “Tri-functional metasurface enhanced with a physically unclonable function,” *Mater. Today* **62**, 51 (2023).
235. W. Zhang *et al.*, “Chameleon-inspired active tunable structural color based on smart skin with multi-functions of structural color, sensing and actuation,” *Mater. Horiz.* **10**, 2024 (2023).
236. M. Dolatyari *et al.*, “Transparent display using a quasi-array of Si-SiO₂ core-shell nanoparticles,” *Sci. Rep.* **9**, 2293 (2019).
237. Q. Fu *et al.*, “Electrically responsive photonic crystals with bistable states for low-power electrophoretic color displays,” *Nat. Commun.* **13**, 7007 (2022).
238. W.-J. Joo *et al.*, “Metasurface-driven OLED displays beyond 10,000 pixels per inch,” *Science* **370**, 459 (2020).
239. G. Lippmann, “La photographie integrale,” *Comptes-Rendus* **146**, 446 (1908).
240. J. You En Chan *et al.*, “Structural color prints combined with microlens arrays for sustainable autostereoscopic displays,” *Mater. Today. Proc.* **70**, 283 (2022).
241. J. Y. E. Chan *et al.*, “High-resolution light field prints by nanoscale 3D printing,” *Nat. Commun.* **12**, 3728 (2021).
242. H. Zhou *et al.*, “Optically controlled dielectric metasurfaces for dynamic dual-mode modulation on terahertz waves,” *Adv. Photonics* **5**, 026005 (2023).
243. X. Wang *et al.*, “Structural colors by synergistic birefringence and surface plasmon resonance,” *ACS Nano* **14**, 16832 (2020).
244. M. Esposito *et al.*, “Symmetry Breaking in oligomer surface plasmon lattice resonances,” *Nano Lett.* **19**, 1922 (2019).
245. F. Zhang *et al.*, “Simultaneous full-color printing and holography enabled by centimeter-scale plasmonic metasurfaces,” *Adv. Sci.* **7**, 1903156 (2020).
246. R. Feng *et al.*, “A modular design of continuously tunable full color plasmonic pixels with broken rotational symmetry,” *Adv. Funct. Mater.* **32**, 2108437 (2022).
247. Y. Jung *et al.*, “Polarization selective color filter based on plasmonic nanograting embedded etalon structures,” *Nano Lett.* **20**, 6344 (2020).
248. J. Cai *et al.*, “Dual-color flexible metasurfaces with polarization-tunable plasmons in gold nanorod arrays,” *Adv. Opt. Mater.* **9**, 2001401 (2021).
249. Y. Ke *et al.*, “Engineering dynamic structural color pixels at microscales by inhomogeneous strain-induced localized topographic change,” *Nano Lett.* **23**, 5520 (2023).
250. H. Wang *et al.*, “Coloured vortex beams with incoherent white light illumination,” *Nat. Nanotechnol.* **18**, 264 (2023).
251. D. Hu *et al.*, “Laser-splashed three-dimensional plasmonic nanovolcanoes for steganography in angular anisotropy,” *ACS Nano* **12**, 9233 (2018).
252. S. So *et al.*, “Multicolor and 3D holography generated by inverse-designed single-cell metasurfaces,” *Adv. Mater.* **35**, 2208520 (2023).
253. Y. Intaravanne *et al.*, “Color-selective three-dimensional polarization structures,” *Light Sci. Appl.* **11**, 302 (2022).
254. Z.-L. Deng *et al.*, “Full-color complex-amplitude vectorial holograms based on multi-freedom metasurfaces,” *Adv. Funct. Mater.* **30**, 1910610 (2020).
255. Q. Wei *et al.*, “Simultaneous spectral and spatial modulation for color printing and holography using all-dielectric metasurfaces,” *Nano Lett.* **19**, 8964 (2019).
256. Q. Dai *et al.*, “A single-celled tri-functional metasurface enabled with triple manipulations of light,” *Adv. Funct. Mater.* **30**, 2003990 (2020).
257. D. Kang *et al.*, “Multispectral imaging with a planar cavity-type metasurface for optical security,” *ACS Appl. Mater. Interfaces* **15**, 29577 (2023).
258. L. Li *et al.*, “Optical metasurfaces for multiplex high-performance grating-type structural colors,” *Opt. Lett.* **48**, 1686 (2023).
259. K. T. P. Lim *et al.*, “Holographic colour prints for enhanced optical security by combined phase and amplitude control,” *Nat. Commun.* **10**, 25 (2019).
260. Y. Bao *et al.*, “Full-colour nanoprint-hologram synchronous metasurface with arbitrary hue-saturation-brightness control,” *Light Sci. Appl.* **8**, 95 (2019).
261. W. Yang *et al.*, “Dynamic bifunctional metasurfaces for holography and color display,” *Adv. Mater.* **33**, 2101258 (2021).
262. I. Kim *et al.*, “Pixelated bifunctional metasurface-driven dynamic vectorial holographic color prints for photonic security platform,” *Nat. Commun.* **12**, 3614 (2021).
263. Y. Hu *et al.*, “3D-Integrated metasurfaces for full-colour holography,” *Light Sci. Appl.* **8**, 86 (2019).
264. H. Sugimoto *et al.*, “Mie resonator color inks of monodispersed and perfectly spherical crystalline silicon nanoparticles,” *Adv. Opt. Mater.* **8**, 2000033 (2020).
265. J. B. Kim *et al.*, “Direct writing of customized structural-color graphics with colloidal photonic inks,” *Sci. Adv.* **7**, eabj8780 (2021).
266. K. Li *et al.*, “Facile full-color printing with a single transparent ink,” *Sci. Adv.* **7**, eabh1992 (2021).
267. J. A. H. P. Sol *et al.*, “Direct ink writing of 4D structural colors,” *Adv. Funct. Mater.* **32**, 2201766 (2022).
268. R. Bi *et al.*, “3D-printed biomimetic structural colors,” *Small* **20**, 2306646 (2023).
269. A. F. Demirörs *et al.*, “Three-dimensional printing of photonic colloidal glasses into objects with isotropic structural color,” *Nat. Commun.* **13**, 4397 (2022).
270. H. Zhang *et al.*, “Stretchable and conductive composite structural color hydrogel films as bionic electronic skins,” *Adv. Sci.* **8**, 2102156 (2021).
271. Y.-J. Quan *et al.*, “Stretchable biaxial and shear strain sensors using diffractive structural colors,” *ACS Nano* **14**, 5392 (2020).
272. F. Lütolf *et al.*, “Low-cost and large-area strain sensors based on plasmonic fano resonances,” *Adv. Opt. Mater.* **4**, 715 (2016).
273. P. Cencillo-Abad *et al.*, “Reusable structural colored nanostructure for powerless temperature and humidity sensing,” *Adv. Opt. Mater.* **11**, 2300300 (2023).
274. C. Jung *et al.*, “Disordered-nanoparticle-based etalon for ultrafast humidity-responsive colorimetric sensors and anti-counterfeiting displays,” *Sci. Adv.* **8**, eabm8598 (2022).
275. B. Ko *et al.*, “Humidity-responsive RGB-pixels via swelling of 3D nanoimprinted polyvinyl alcohol,” *Adv. Sci.* **10**, 2204469 (2023).

276. K. Kang *et al.*, "Self-powered gas sensor based on a photovoltaic cell and a colorimetric film with hierarchical micro/nanostructures," *ACS Appl. Mater. Interfaces* **12**, 39024 (2020).
277. D. P. Langley *et al.*, "Optical chemical barcoding based on polarization controlled plasmonic nanopixels," *Adv. Funct. Mater.* **28**, 1704842 (2018).
278. C. Burel *et al.*, "Plasmonic elastic capsules as colorimetric reversible pH-microsensors," *Small* **16**, 1903897 (2020).
279. J. Ho *et al.*, "Miniaturizing color-sensitive photodetectors via hybrid nanoantennas toward submicrometer dimensions," *Sci. Adv.* **8**, eadd3868 (2022).
280. D. Tua *et al.*, "Imaging-based intelligent spectrometer on a plasmonic rainbow chip," *Nat. Commun.* **14**, 1902 (2023).
281. M. Qin *et al.*, "A rainbow structural-color chip for multisaccharide recognition," *Angew. Chem. Int. Ed.* **55**, 6911 (2016).
282. L. Zheng *et al.*, "A microfluidic colorimetric biosensor for rapid detection of *Escherichia coli* O157:H7 using gold nanoparticle aggregation and smart phone imaging," *Biosens. Bioelectron.* **124-125**, 143 (2019).
283. C. Zhou *et al.*, "Optofluidic sensor for inline hemolysis detection on whole blood," *ACS Sens.* **3**, 784 (2018).
284. J. L. Montaña-Priede *et al.*, "Robust rules for optimal colorimetric sensing based on gold nanoparticle aggregation," *ACS Sens.* **8**, 1827 (2023).
285. F. Fu *et al.*, "Bioinspired living structural color hydrogels," *Sci. Rob.* **3**, eaar8580 (2018).
286. M. Alafeef *et al.*, "RNA-extraction-free nano-amplified colorimetric test for point-of-care clinical diagnosis of COVID-19," *Nat. Protoc.* **16**, 3141 (2021).
287. P. Moitra *et al.*, "Selective naked-eye detection of SARS-CoV-2 mediated by N gene targeted antisense oligonucleotide capped plasmonic nanoparticles," *ACS Nano* **14**, 7617 (2020).
288. J.-H. Choi *et al.*, "CRISPR-Cas12a-based nucleic acid amplification-free DNA biosensor via Au nanoparticle-assisted metal-enhanced fluorescence and colorimetric analysis," *Nano Lett.* **21**, 693 (2021).
289. E. Balaur *et al.*, "Colorimetric histology using plasmonically active microscope slides," *Nature* **598**, 65 (2021).
290. T. M. Nguyen *et al.*, "Multiarray biosensor for diagnosing lung cancer based on gap plasmonic color films," *ACS Sens.* **8**, 167 (2023).
291. F. Yesilkoy *et al.*, "Ultrasensitive hyperspectral imaging and bio-detection enabled by dielectric metasurfaces," *Nat. Photonics* **13**, 390 (2019).
292. Z. Zhao *et al.*, "Bioinspired heterogeneous structural color stripes from capillaries," *Adv. Mater.* **29**, 1704569 (2017).
293. T. Chen and B. M. Reinhard, "Assembling color on the nanoscale: multichromatic switchable pixels from plasmonic atoms and molecules," *Adv. Mater.* **28**, 3522 (2016).
294. L. Wang *et al.*, "Large area plasmonic color palettes with expanded gamut using colloidal self-assembly," *ACS Photonics* **3**, 627 (2016).
295. Z. Chen *et al.*, "Antibacterial structural color hydrogels," *ACS Appl. Mater. Interfaces* **9**, 38901 (2017).
296. R. H. Siddique *et al.*, "Scalable and controlled self-assembly of aluminum-based random plasmonic metasurfaces," *Light Sci. Appl.* **6**, e17015 (2017).
297. R. M. Parker *et al.*, "The self-assembly of cellulose nanocrystals: hierarchical design of visual appearance," *Adv. Mater.* **30**, 1704477 (2018).
298. T. S. Kustandi *et al.*, "Mimicking domino-like photonic nanostructures on butterfly wings," *Small* **5**, 574 (2009).
299. A. F. Kaplan *et al.*, "Multilayer pattern transfer for plasmonic color filter applications," *J. Vac. Sci. Technol. B* **28**, C6O60 (2010).
300. A. F. Kaplan *et al.*, "High efficiency resonance-based spectrum filters with tunable transmission bandwidth fabricated using nanoimprint lithography," *Appl. Phys. Lett.* **99**, 143111 (2011).
301. K.-T. Lee *et al.*, "Subwavelength nanocavity for flexible structural transmissive color generation with a wide viewing angle," *Optica* **3**, 1489 (2016).
302. K.-T. Lee *et al.*, "Highly efficient colored perovskite solar cells integrated with ultrathin subwavelength plasmonic nanoresonators," *Sci. Rep.* **7**, 10640 (2017).
303. B. M. Gawlik *et al.*, "Structural coloration with hourglass-shaped vertical silicon nanopillar arrays," *Opt. Express* **26**, 30952 (2018).
304. S. Checcucci *et al.*, "Multifunctional metasurfaces based on direct nanoimprint of titania sol-gel coatings," *Adv. Opt. Mater.* **7**, 1801406 (2019).
305. H. Zheng *et al.*, "Multichannel meta-imagers for accelerating machine vision," *Nat. Nanotechnol.* (2024).
306. S. H. Ahn and L. J. Guo, "High-speed roll-to-roll nanoimprint lithography on flexible plastic substrates," *Adv. Mater.* **20**, 2044 (2008).
307. S. H. Ahn and L. J. Guo, "Large-area roll-to-roll and roll-to-plate nanoimprint lithography: a step toward high-throughput application of continuous nanoimprinting," *ACS Nano* **3**, 2304 (2009).
308. P. Somers *et al.*, "The physics of 3D printing with light," *Nat. Rev. Phys.* **6**, 99 (2023).
309. Q. Geng *et al.*, "Ultrafast multi-focus 3-D nano-fabrication based on two-photon polymerization," *Nat. Commun.* **10**, 2179 (2019).
310. T. Mori *et al.*, "Pick and place process for uniform shrinking of 3D printed micro- and nano-architected materials," *Nat. Commun.* **14**, 5876 (2023).
311. Y. Liu *et al.*, "Structural color three-dimensional printing by shrinking photonic crystals," *Nat. Commun.* **10**, 4340 (2019).
312. H. Liu *et al.*, "High-order photonic cavity modes enabled 3D structural colors," *ACS Nano* **16**, 8244 (2022).
313. J. Bae *et al.*, "Three-dimensional printing of structural color using a femtoliter meniscus," *ACS Nano* **17**, 13584 (2023).
314. M. del Pozo *et al.*, "Direct laser writing of four-dimensional structural color microactuators using a photonic photoresist," *ACS Nano* **14**, 9832 (2020).
315. J. S. Llorens *et al.*, "Light-based 3D printing of complex-shaped photonic colloidal glasses," *Adv. Mater.* **35**, 2302868 (2023).
316. Y. Zhang *et al.*, "Continuous resin refilling and hydrogen bond synergistically assisted 3D structural color printing," *Nat. Commun.* **13**, 7095 (2022).
317. H. Wang *et al.*, "Optical fireworks based on multifocal three-dimensional color prints," *ACS Nano* **15**, 10185 (2021).
318. A. Kumar *et al.*, "Phototunable chip-scale topological photonics: 160 Gbps waveguide and demultiplexer for THz 6G communication," *Nat. Commun.* **13**, 5404 (2022).
319. G. Giribaldi *et al.*, "Compact and wideband nanoacoustic pass-band filters for future 5G and 6G cellular radios," *Nat. Commun.* **15**, 304 (2024).
320. X. Lin *et al.*, "All-optical machine learning using diffractive deep neural networks," *Science* **361**, 1004 (2018).
321. J. Li *et al.*, "Spectrally encoded single-pixel machine vision using diffractive networks," *Sci. Adv.* **7**, eabd7690 (2021).
322. F. Zangeneh-Nejad *et al.*, "Analogue computing with metamaterials," *Nat. Rev. Mater.* **6**, 207 (2021).
323. J. Li *et al.*, "Massively parallel universal linear transformations using a wavelength-multiplexed diffractive optical network," *Adv. Photonics* **5**, 016003 (2023).
324. C.-Y. Shen *et al.*, "Multispectral quantitative phase imaging using a diffractive optical network," *Adv. Intell. Syst.* **5**, 2300300 (2023).